A mathematical model of a direct-fired continuous strip annealing furnace

authored by **S. Strommer, M. Niederer, A. Steinboeck, and A. Kugi**

and published in *International Journal of Heat and Mass Transfer.*

Read more ACIN papers or get this document:

http://www.acin.tuwien.ac.at/literature

Contact:

Automation and Control Institute (ACIN)	Internet: www.acin.tuwien.ac.at
Vienna University of Technology	E-mail: office@acin.tuwien.ac.at
Gusshausstrasse 27-29/E376	Phone: +43 1 58801 37601
1040 Vienna, Austria	Fax: +43 1 58801 37699

A mathematical model of a direct-fired continuous strip annealing furnace

S. Strommer*, M. Niederer, A. Steinboeck, A. Kugi

Automation and Control Institute, Vienna University of Technology, Gusshausstrasse 27–29, 1040 Wien, Austria

Abstract

A mathematical model of a direct-fired continuous strip annealing furnace is developed. The first-principle model uses the heat balance to describe the dynamic behavior of the strip and the rolls. The mass and the enthalpy balance are employed to calculate the mass, the composition, and the temperature of the flue gas. The heat conduction equation of the furnace wall is discretized by means of the Galerkin method. Furthermore, the convective and radiative heat transfer interconnect all submodels of the furnace. For the calculation of the radiative heat transfer, the zone method is utilized. Finally, the assembled model is reduced by applying the singular perturbation method. A comparison of simulation results with measurement data from a real plant demonstrates the accuracy of the reduced model. Moreover, due to the moderate computational effort, the model is suitable for real-time applications in control and dynamic optimization.

Key words: Direct-fired strip annealing furnace, fuel-rich combustion, water-gas-shift reaction, balance equation, Galerkin method, convective and radiative heat exchange

1. Introduction

1.1. Objective

In continuous annealing furnaces, see, e.g., [25, 26], metal strip products are heat-treated. The direct-fired strip annealing furnace considered in this paper is part of a hot-dip galvanizing line at voestalpine Stahl GmbH, Linz, Austria. A schematic diagram of this furnace is depicted in Fig. 1. The galvanizing line also contains an indirect-fired furnace (IFF) [25], which comes right after the direct-fired furnace but will not be detailed in this paper. Based on metallurgical requirements the strip has to be heated from ambient temperature along a predefined heating curve to a desired target temperature at the outlet of the furnace.

Temperature control of strip annealing furnaces is a challenging task, in particular in transient operating situations when there are changes in the strip dimensions (width, thickness), the velocity or the steel grade. A further difficulty for temperature control is that the strip temperature can only be measured at a very few discrete points mostly by means of pyrometers. Moreover, due to their high energy consumption, continuous strip annealing furnaces are important cost drivers of strip processing lines. This is why, apart from the product quality, minimum energy consumption, minimum flue gas emissions and minimum operating costs constitute further major control objectives. These objectives demand the application of advanced (nonlinear) control and optimization methods [2, 3, 23], which systematically take into account the essential nonlinearities, the dynamical interactions and the delays of the overall system. For this, tailored mathematical models have to be developed, which constitute a reasonable compromise between accuracy and complexity and serve as a basis for real-time control and optimization.

*Corresponding author. *Tel.:* +43 1 58801 376290, *fax:* +43 1 58801 37699.
Email address: strommer@acin.tuwien.ac.at (S. Strommer)

Nomenclature

Latin symbols

Bi	Biot number
c_p	specific heat capacity
d	thickness
d_r	diameter of the roll
H	enthalpy of the flue gas
$\dot{H}$	enthalpy flow of the flue gas
h	absolut (specific) enthalpy
h_c	convection heat transfer coefficient
$\tilde{h}_l$	latent heat
J	cost function
K	attenuation coefficient
k	thermal conductivity
M	mass
$\dot{M}$	mass flow
$\bar{M}$	molar mass
$\mathbf{M}_q$	Local heat flux mapping matrix
$\mathbf{M}_T$	Temperature mapping matrix
N	number of volume zones
Nu	Nusselt number
N_s	number of surface sections
$\bar{N}_s, \tilde{N}_s$	number of finite sections in Eulerian and Lagrangian coordinates
N_g	number of subvolumes
Pr	Prandtl number
$\mathbf{P}$	radiation mapping matrix
p	pressure
$\dot{Q}$	heat flow
$\dot{\mathbf{Q}}$	vector of heat flows
$\dot{q}, \check{\tilde{q}}$	heat flux in Eulerian and Lagrangian coordinates
$\dot{\mathbf{q}}$	vector of heat fluxes
Re	Reynolds number
R_{con}	thermal contact resistance
R	specific gas constant
S	surface area
$\mathbf{S}$	vector of surface areas
T	temperature

$\tilde{T}$	temperature in Lagrangian coordinates
$\mathbf{T}$	vector of temperatures
t_e, t_b	start and end time
$\mathbf{u}$	input vector
V	volume
v	trial function
v_s	strip and roll velocity
x, y, z	Eulerian coordinates
$\tilde{x}, \tilde{y}, \tilde{z}$	Lagrangian coordinates
$\mathbf{x}$	state vector
$\mathbf{z}_1, \mathbf{z}_2$	state vectors of the fast and slow subsystem
$\check{\mathbf{z}}_1, \check{\mathbf{z}}_2$	state vectors of the quasi-steady-state system

Greek symbols

α	flow coefficient
χ	number of moles
$\Delta \tilde{h}_s$	sensible heat
ε	emissivity coefficient
λ	excess air coefficient
μ	dynamic viscosity
ρ	mass density
Δt_k	sampling time
$\tilde{\zeta}$	mass fraction
$\Delta z, \Delta \tilde{z}$	length of a finite section in Eulerian and Lagrangian coordinates

Subscripts

g	flue gas
r	roll
s	strip
v	volume
w	wall

Superscripts

a	air
cb	combustion
f	fuel
in	incoming
out	outgoing

1.2. Direct-fired furnace

The furnace considered in this analysis (cf. Fig. 1) contains approximately 50 m strip, which moves at velocities in the range of $1.5 - 3\,\text{m/s}$ through the furnace. The maximum strip thickness is $1.2\,\text{mm}$ and the width can be up to $1.7\,\text{m}$. The insulating materials of the furnace walls are refractory and the guiding rolls are made of high temperature alloy. In essence, the hot flue gas streams in the opposite direction of the strip through the furnace and, therefore, the furnace may be considered as a counter-flow heat exchanger. At the air lock 1 (right side of Fig. 1), which represents the interface between the direct- and the indirect-fired furnace,
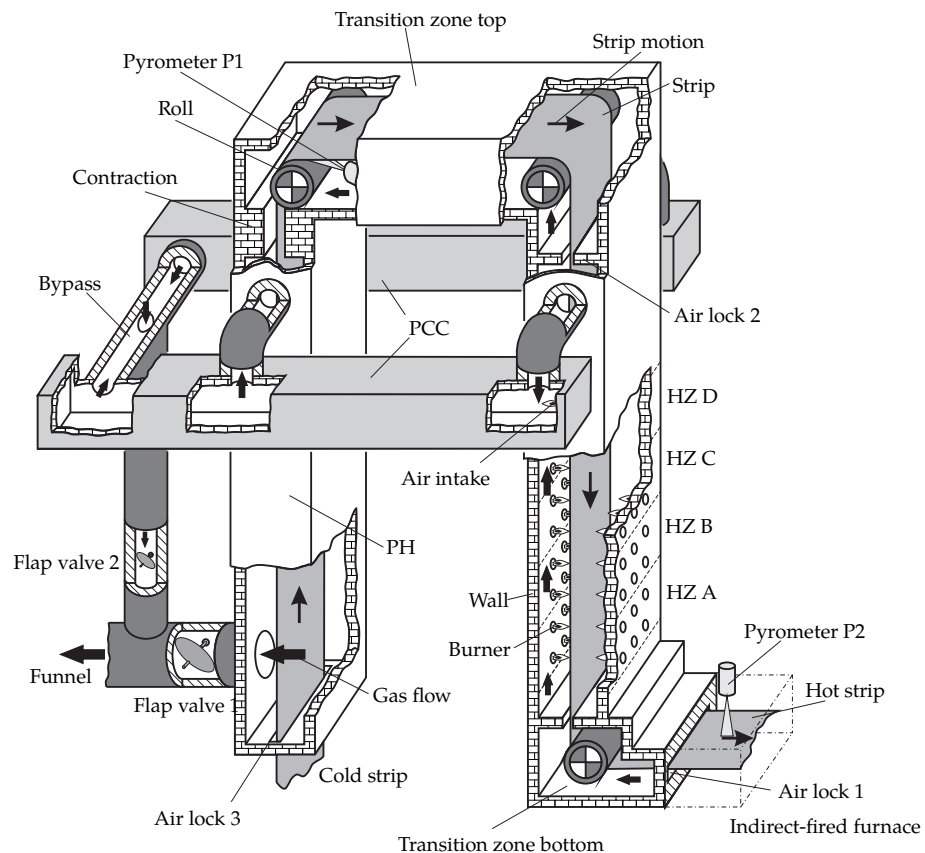
2

Figure 1: Direct-fired strip annealing furnace.

inert gas from the indirect-fired furnace enters the direct-fired furnace. The inert gas atmosphere in the indirect-fired furnace is used to avoid scale formation. Between the air lock 1 and the air lock 2, there are four heating zones (HZ A – D), each equipped with a set of burners supplied by natural gas. For quality reasons, the strip must not be oxidized, which is why a substoichiometric combustion has to be ensured. Thus, the flue gas that leaves the heating zone HZ D contains unburnt gas, which is oxidized in a post combustion chamber (PCC) by adding fresh air (cf. air intake in Fig. 1). The section between the air lock 2 and the contraction is referred to as transition zone top. A small amount of the flue gas flows through the air lock 2, which can be considered as an orifice connecting the heating zones and the transition zone top. However, most of the flue gas leaves the HZ D

through a bypass which includes the PCC. After burning the remaining combustible components in the PCC, the flue gas does not contain any oxidizable or potentially harmful elements and may be released into the environment or further used, e.g., for preheating the combustion air or the strip (cf. Fig. 1).

The flap valve 2, which works like an orifice, controls the gas flow from the PCC to the so-called bypass. This duct allows to bypass flue gas (typically a small amount) directly into the funnel. However, the majority of the burnt flue gas flows into the furnace section between the contraction and the air lock 3, which is called preheater (PH). There, the remaining sensible heat of the flue gas is used for preheating the strip. The air lock 3 can also be considered as an orifice, where depending on the pressure conditions flue gas leaves the furnace or fresh

air flows into the PH. Generally, the mass flow of gas through the air lock 3 is rather small. The flue gas from the PH leaves the furnace through the funnel. A suction fan (not shown in Fig. 1) controls the suction pressure to a value less than the atmospheric pressure, which makes the flue gas to stream to the funnel. Moreover, a recuperator (not shown in Fig. 1) utilizes the remaining enthalpy of the hot flue gas to preheat the combustion air for the burners in the HZ C and HZ D.

1.3. Existing models

A large number of different approaches for modeling a strip annealing furnace can be found in the literature.

One way of setting up such a furnace model is the use of computational fluid dynamics (CFD), which allows high-resolution evaluations of the heat and mass flows in the furnace [4, 9, 10]. CFD models typically take into account the combustion process, the furnace geometry, and the energy exchange between the strip, the flue gas, the furnace walls, and the rolls. Due to their complexity and high dimensions, CFD models are usually not directly suitable for control design and real-time applications. The use of CFD is more common in the design of new furnaces and in off-line studies.

For model-based control applications, physical or empirical models are required that are computationally inexpensive. The models must be executable in real-time, which is sometimes ensured by using empirical models, see, e.g., [45]. A semi-analytic model of a strip annealing furnace is presented in [46]. This mathematical model consists of a dynamic and a static part. The dynamic model is derived from the heat balance equation and the static model is based on curve-fitting approximation of the calculated strip temperature obtained by heat transfer calculation. For this approach, a physical interpretation of the parameters is rather difficult.

Furthermore, linearized models are often used to ensure real-time capability, see, e.g., [3, 10, 39]. Clearly, these models neglect nonlinear material parameters and the 4th–powers occurring in radiative heat transfer relations.

First-principle models typically rely on balance equations and constitutive equations which include the most important heat transfer mecha-

nisms, i.e., convection, conduction, and thermal radiation. Heat convection and conduction are local phenomena, whereas radiation is a global phenomenon. Depending on the composition of the flue gas, it must be considered as a participating medium in the radiative interaction, see, e.g., [2, 5, 13, 16, 17, 18, 26, 27, 30, 31, 40]. In [43, 44], a first-principle model is developed for a pusher-typ slab reheating furnace, where the gaseous medium is participating in thermal radiation. The mathematical model is based on mass, enthalpy, and heat balances. A reduced mathematical model of the pusher-typ slab reheating furnace was developed in [33]. This reduced model has been used for a model-based controller design in [35].

The properties of the flue gas are influenced by the combustion of the natural gas and further chemical reactions, e.g., the water-gas-shift reaction [2, 5, 8, 19, 28]. This reversible reaction, which depends on the flue gas temperature, is relevant for modeling the flue gas in the heating zones of the considered furnace because it defines the respective chemical equilibrium.

Although there exist several models for direct-fired furnaces in the literature, they may not be directly applied to the furnace considered in this work, mainly due to the following reasons:

- Generally, the existing mathematical models cannot be tailored to the specific furnace due to the high complexity.
- In the considered furnace, natural gas is burnt fuel-rich and, hence, the gas is a participating medium. Therefore, the flue gas plays a significant role in the current mathematical model.
- Typically, the combustion process is neglected [2, 5, 26, 39, 40, 45, 46]. However, a consideration of the combustion is relevant for the characterization of the chemical reactions and the composition of the flue gas. Equilibrium equations, which depend on the local flue gas temperature [8, 19, 28], have a significant influence on the composition of the flue gas and thus on the heat input.
- By neglecting the gas combustion, the mathematical model cannot capture the impact of fluctuations of the excess air coefficient and, thus, also the corresponding heat input.
- In the PCC, the oxidizable products are burnt. For this conversion, the composition of the flue

4

gas should be exactly known because otherwise a wrong heat input may be predicted.

1.4. Contents

The paper is structured as follows: In Sec. 2, the mathematicel model of the direct-fired furnace is derived with a focus on the heating of the strip. Moreover, the gas temperature, the gas flow, and the composition of the flue gas in the furnace are discussed and the underlying chemical reactions are presented. The continuous-time state space model of the whole direct-fired furnace finally consists of the submodels for the walls, the strip, the flue gas, and the guiding rolls, which are connected via convective and radiative heat transfer. In Sec. 3, the model is reduced by means of the singular perturbation theory and the time domain is discretized. The accuracy of the proposed mathematical model is verified in Sec. 4 by comparing simulation and measurement results.

2. Mathematical model

The mathematical model of the considered furnace is based on balance equations, i.e., mass and enthalpy balances for the flue gas and heat balances for the rolls, the walls, and the strip. Basically, the furnace is a distributed-parameter system. To simplify the analysis, the furnace is divided into N volume zones, where the zones HZ A to HZ D are equipped with burners (see Fig. 1). The composition of the flue gas is mainly controlled by the combustion. The flue gas interacts with the surrounding surfaces (strip, walls, and rolls) by radiation and convection.

2.1. Flue gas

The flue gas generally consists of reaction products from the substoichiometric combustion of natural gas in the heating zones. However, it also contains inert gas from the indirect-fired furnace, which enters the direct-fired furnace at the air lock 1. The flue gas thus contains the components carbon dioxide, carbon monoxide, water, hydrogen, oxygen, and nitrogen, which are summerized in the set $\mathcal{S} = \{CO_2, CO, H_2O, H_2, O_2, N_2\}$. Due to the atomic and molecular spectra of these components, it is necessary to consider the flue gas as a participating medium in the analysis of radiative heat

transfer [27].

For modeling the gas flow, each of the N volume zones is considered as a well-stirred reactor and it is assumed that the gas flow does not change its direction. Fig. 1 schematically shows the geometry of the direct-fired furnace. Considering this geometry in detail would entail inordinate complexity of the mathematical model, which is why a simplified furnace geometry will be used in the following derivation. The furnace is considered as a tube and divided into $N = 24$ volume zones (VZ), see Fig. 2.

Fig. 3 shows the mass and energy flows of volume zone i, where the flue gas is characterized by the mass M_i and the temperature $T_{g,i}$. The corresponding mass and energy balances will be detailed in Sec. 2.1.3 and Sec. 2.1.4, respectively. The energy exchange between the flue gas and the surrounding surfaces is defined by the net heat flow $\dot{Q}_{s,i}$ into the strip and $\dot{Q}_{w,i}$ into the furnace wall. These heat flows include both convective and radiative heat transfer (cf. Sec. 2.5 and Sec. 2.6).

2.1.1. Gas flow

The gas flow is induced by a pressure gradient which is feedback controlled to ensure a defined volume flow. The pressure decreases from the air lock 1 to the funnel and is controlled by flap valves and a suction fan (cf. Fig. 4). The suction fan is located in the funnel and has to make sure that the flue gas leaves the furnace towards the funnel.

The three air locks have all the same design as indicated in Fig. 4. Each air lock has two gaps on both sides of the strip, namely between the roll and the strip and between the roll and the wall. The gas flow through the air lock relies on the existing pressure gradient ($p_1 > p_2$) and the velocity v_s of the strip and the roll surface. This gas flow can be modeled by means of the Navier-Stokes-equation [6], however, a fairly good approximation is given by the Couette flow. With this, the unknown gas flows $\dot{M}_{21}^{air}$ and $\dot{M}_{10}^{in}$ can be determined (cf. Fig. 4).

At the bottom of the PH, the flue gas leaves the furnace through the flap valve 1 into the funnel. The two flap valves 1 and 2 are inversely controlled, which means that the total opening area of both valves is kept constant.

At the interface between the transition zone top and the PH, the main duct has a contraction. Moreover, the entry and the exit of the PCC also behave

5
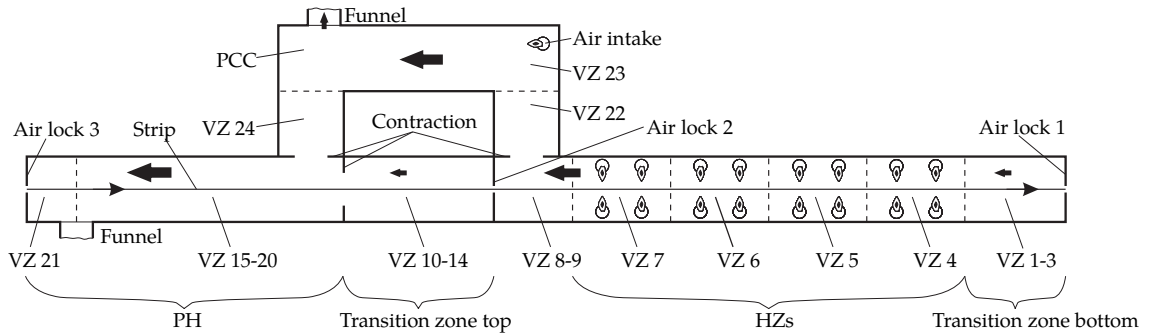
Figure 2: Geometrically simplified volume zones of the direct-fired furnace.
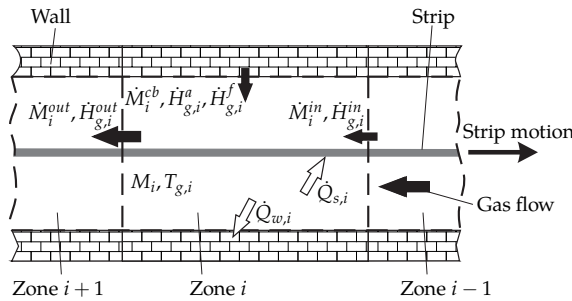
Figure 3: Volume zone i with mass and energy flows.

like a contraction. The mass flow through a contraction can be found from the standard orifice formula [20]

$$\dot{M}^{or} = \alpha^{or} A^{or} \sqrt{2\rho_g \Delta p}. \tag{1}$$

Here, Δp describes the local pressure difference, α^{or} the flow coefficient, and A^{or} the opening area of the respective orifice. In [20], an approximation for α^{or} is given in the form $\alpha^{or} = 0.6 + 0.41(A^{or}/A^{fu})^2$, where A^{fu} defines the cross sectional area of the main duct of the furnace.

To determine the mass flow through an orifice, the pressure difference Δp needs to be known. In the considered furnace, the pressure is only measured at two positions, i.e., at the bottom of the HZs (p_{HZ}) and at the bottom of the PH (p_{PH}) (cf. Fig 4). Based on these two measurements and the knowledge of the mass flow $\dot{M}_1^{in}$ of the inert gas from the indirect-fired furnace all other mass flows and pressures in Fig. 4 can be calculated in a straight forward way.

Figure 4: Gas flows in the direct-fired furnace.

6

2.1.2. Chemical reactions

In the HZs, fuel reacts with air at the nozzles of the burners and energy is released into the respective zone. The energy which evolves from the burning of the remaining combustible components in the PCC additionally heats the flue gas. In the following, the combustion reactions in the HZs and in the PCC are analyzed in more detail.
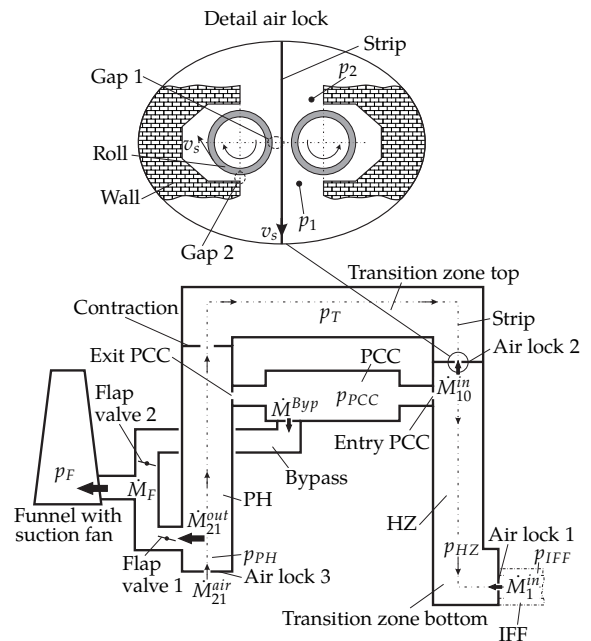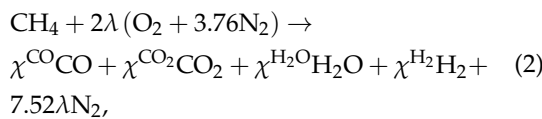
Heating zones. The four HZs are represented in Fig. 2 by the volume zones $4 - 7$. The burners are operated with air and natural gas, which mainly consists of methane (CH_4). Considering only CH_4 in the model is acceptable because the CH_4-concentration of the natural gas used in the considered furnace always exceeds 96% and the latent heat of the natural gas is almost equal to that of pure CH_4. The combustion is controlled to be fuel-rich [41], which ensures the absence of O_2 and thus avoids the formation of scale. The reaction equation of the fuel-rich combustion of CH_4 reads as

$$CH_4 + 2\lambda\left(O_2 + 3.76 N_2\right) \rightarrow$$
$$\chi^{CO} CO + \chi^{CO_2} CO_2 + \chi^{H_2O} H_2O + \chi^{H_2} H_2 + \quad (2)$$
$$7.52\lambda N_2,$$

where $\chi^{H_2O}, \chi^{H_2} \in [0,2]$ and $\chi^{CO_2}, \chi^{CO}, \lambda \in [0,1]$ refer to the corresponding number of moles, $1/\lambda$ is the equivalence ratio, and λ is the excess air coefficient. In the considered furnace, λ is chosen for each HZ according to a generally constant set-point value. For the model, λ thus serves as an input. Stoichiometric relations yield

$$C: \quad 1 = \chi^{CO} + \chi^{CO_2} \quad (3a)$$

$$H: \quad 4 = 2\chi^{H_2O} + 2\chi^{H_2} \quad (3b)$$

$$O: \quad 4\lambda = \chi^{H_2O} + 2\chi^{CO_2} + \chi^{CO}. \quad (3c)$$

The fourth equation required to compute $\chi^{H_2O}, \chi^{H_2}, \chi^{CO_2}$, and χ^{CO} can be obtained by considering the so-called water-gas-shift reaction [29, 41]

$$CO + H_2O \rightleftharpoons H_2 + CO_2. \quad (4)$$
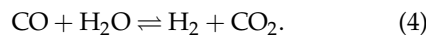
It depends on the local gas temperature $T_{g,i}$ and reaches an equilibrium if

$$\frac{\chi^{CO}\chi^{H_2O}}{\chi^{CO_2}\chi^{H_2}} = e^{4.33 - \frac{4577.8\,K}{T_{g,i}}} \quad (5)$$

is satisfied [8, 28].

For the model, it is justifiable to consider that all reactions (cf. (2) and (4)) attain their equilibrium instantaneously, i.e., they are considered as quasi-stationary.

Let $\dot{M}_i^{\nu,cb}$ be the mass flow of the gas component $\nu \in \mathcal{S}$ that enters the furnace through the burners in zone i after the combustion has occurred. The molar mass of the component $\nu \in \mathcal{S}$ is given by $\bar{M}^\nu$, which implies that the mass fraction of the combustion product $\nu \in \mathcal{S}$ reads as

$$\xi_i^{\sigma,cb} = \frac{\zeta \bar{M}^\sigma}{\sum_{\nu \in \mathcal{S}} \chi^\nu \bar{M}^\nu}, \quad (6)$$

with $(\sigma,\zeta) \in \left\{ (H_2O, \chi^{H_2O}), (H_2, \chi^{H_2}), (CO_2, \chi^{CO_2}), (CO, \chi^{CO}), (N_2, \lambda 7.52) \right\}$. Based on (6), the mass flow of the component $\nu \in \mathcal{S}$ follows as

$$\dot{M}_i^{\nu,cb} = \xi_i^{\nu,cb}(\dot{M}_i^f + \dot{M}_i^a), \quad (7)$$

with the mass flow of fuel $\dot{M}_i^f$ into the burners of zone i and the corresponding mass flow of air $\dot{M}_i^a$, which is coupled to λ and $\dot{M}_i^f$ in the following way

$$\dot{M}_i^a = \frac{2(\bar{M}^{O_2} + 3.76\bar{M}^{N_2})}{\bar{M}^{CH_4}}\lambda \dot{M}_i^f. \quad (8)$$

Here $\bar{M}^{O_2}$, $\bar{M}^{N_2}$ and $\bar{M}^{CH_4}$ denote the molar mass of O_2, N_2 and CH_4, respectively.

Post combustion chamber. As shown in Fig. 2, the volume zone 23 conceptually represents both symmetrical PCCs (cf. Fig. 1).

In the PCC, the remaining amounts of H_2 and CO are burnt according to the combustion reactions

$$CO + \frac{1}{2}\left(O_2 + 3.76 N_2\right) \rightarrow CO_2 + 1.88 N_2, \quad (9a)$$

$$H_2 + \frac{1}{2}\left(O_2 + 3.76 N_2\right) \rightarrow H_2O + 1.88 N_2. \quad (9b)$$
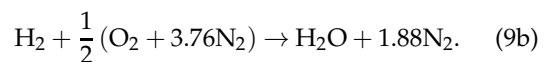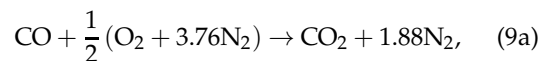
Based on these reaction equations and the bulk flows of carbon monoxide $\dot{M}_{23}^{in,CO}$ and hydrogen $\dot{M}_{23}^{in,H_2}$ into the PCC, the necessary amount of O_2 for an ideal combustion can be calculated as

$$\dot{M}_{23}^{O_2,reac} = \bar{M}^{O_2}\left(\frac{\dot{M}_{23}^{in,CO}}{2\bar{M}^{CO}} + \frac{\dot{M}_{23}^{in,H_2}}{2\bar{M}^{H_2}}\right). \quad (10)$$

7

Generally, more O_2 than necessary according to (10) is supplied to the PCC, i.e., the reaction is controlled to be leaner than stoichiometric and the flue gas leaving the PCC towards the PH contains excess oxygen. The mass flow of excess oxygen $\dot{M}_{23}^{O_2,cb}$ thus reads as

$$\dot{M}_{23}^{O_2,cb} = \frac{\bar{M}^{O_2}}{\bar{M}^{O_2} + 3.76\bar{M}^{N_2}}\dot{M}_{23}^{a} - \dot{M}_{23}^{O_2,reac}, \quad (11)$$

where $\dot{M}_{23}^{a}$ is the total mass flow of fresh air into the PCC. The mass flows $\dot{M}_{23}^{CO_2,cb}$ and $\dot{M}_{23}^{H_2O,cb}$ define the amount of H_2O and CO_2 generated by the chemical reaction (9) in the PCC. Based on (9), it follows that

$$\dot{M}_{23}^{CO_2,cb} = \frac{\bar{M}^{CO_2}}{\bar{M}^{CO}}\dot{M}_{23}^{in,CO}, \quad (12a)$$

$$\dot{M}_{23}^{H_2O,cb} = \frac{\bar{M}^{H_2O}}{\bar{M}^{H_2}}\dot{M}_{23}^{in,H_2}. \quad (12b)$$

2.1.3. The mass of the flue gas

The mass balance is used to determine the mass of the flue gas in each zone i. As mentioned earlier, a plug flow is assumed for the bulk motion of the flue gas. Generally, the mass flow $\dot{M}_i^{in} = \dot{M}_{i-1}^{out}$ enters and the mass flow $\dot{M}_i^{out}$ leaves zone i (cf. Fig. 3). In the zones 4 – 7, the extra mass flow $\dot{M}_i^{cb} = \sum_{\nu \in \mathcal{S}}\dot{M}_i^{\nu,cb} = \dot{M}_i^{f} + \dot{M}_i^{a}$ enters the volume through the burners. In the PCC (volume zone 23), the extra air inflow $\dot{M}_{23}^{cb}$ has to be added. In all other zones $\dot{M}_i^{cb} = 0$. Hence, the mass balance for zone i reads as

$$\frac{dM_i}{dt} = \dot{M}_i^{in} + \dot{M}_i^{cb} - \dot{M}_i^{out} \quad (13a)$$

$$\frac{dM_i^{\nu}}{dt} = \dot{M}_i^{\nu,in} + \dot{M}_i^{\nu,cb} - \dot{M}_i^{\nu,out} \quad \forall \nu \in \mathcal{S} \quad (13b)$$

for the gas mixture and the individual components, respectively. In (13), M_i defines the mass and M_i^{ν} characterizes the mass of the component $\nu \in \mathcal{S}$ of the flue gas in zone i. The mass flows $\dot{M}_i^{\nu,cb}$ are exogenous system inputs. The values $\dot{M}_i^{\nu,in}$ are known from upstream volume zones. The following shows how $\dot{M}_i^{out}$ and consequently also $\dot{M}_i^{\nu,out} = \xi_i^{\nu}\dot{M}_i^{out}$ can be computed. The mass frac-

tion of a component ν can be calculated as

$$\xi_i^{\nu} = \frac{M_i^{\nu}}{M_i}, \quad (14)$$

where

$$M_i = \sum_{\nu \in \mathcal{S}} M_i^{\nu} \quad \text{and} \quad \sum_{\nu \in \mathcal{S}} \xi_i^{\nu} = 1. \quad (15)$$

The bulk flow of the component $\nu \in \mathcal{S}$ into the volume zone i reads as $\dot{M}_i^{\nu,in} = \xi_{i-1}^{\nu}\dot{M}_{i-1}^{out}$. Moreover, $\dot{M}_i^{\nu,cb} = \xi_i^{\nu,cb}\dot{M}_i^{cb}$ defines the mass flow of the combustion product $\nu \in \mathcal{S}$ into the volume. The total differential of (14) yields $dM_i^{\nu} = M_i d\xi_i^{\nu} + dM_i\xi_i^{\nu}$. In view of (13b), it thus follows that

$$M_i \frac{d\xi_i^{\nu}}{dt} = \dot{M}_{i-1}^{out}\left(\xi_{i-1}^{\nu} - \xi_i^{\nu}\right) + \dot{M}_i^{cb}\left(\xi_i^{\nu,cb} - \xi_i^{\nu}\right)$$
$$\forall \nu \in \mathcal{S}. \quad (16)$$

This characterizes the concentration ξ_i^{ν} of the component ν in the volume zone i.

Because the pressure p in the furnace is feedback controlled by means of flap valves (cf. Fig. 4) in order to follow generally constant set-point values, the assumption $dp/dt = 0$ is justified. The ideal gas law

$$pV_i = M_i T_{g,i}\sum_{\nu \in \mathcal{S}} R^{\nu}\xi_i^{\nu} \quad (17)$$

describes the nexus between the mass M_i and the temperature $T_{g,i}$ of the flue gas in zone i. Here V_i represents the volume of zone i and R^{ν} is the specific gas constant of the component ν. In this context, it is assumed that all gaseous media behave like an ideal gas. The time derivative of (17) reads as

$$\frac{dM_i}{dt} = -M_i\left(\frac{1}{T_{g,i}}\frac{dT_{g,i}}{dt} + \frac{1}{\sum_{\nu \in \mathcal{S}} R^{\nu}\xi_i^{\nu}}\sum_{\nu \in \mathcal{S}} R^{\nu}\frac{d\xi_i^{\nu}}{dt}\right). \quad (18)$$

Inserting this expression into (13a) allows the computation of the unknown mass flows $\dot{M}_i^{out}$ and $\dot{M}_i^{\nu,out} = \xi_i^{\nu}\dot{M}_i^{out}$.

2.1.4. The flue gas temperature

The flue gas temperature is required in each volume zone i to determine the heat transfer. The flue gas temperature can be computed from the en-

8

thalpy balance (first law of thermodynamics, see, e.g., [29]). The change of the enthalpy $H_{g,i}$ of the gas in volume zone $i = 1, ..., N$ is given by

$$\frac{\mathrm{d}H_{g,i}}{\mathrm{d}t} = \dot{H}_{g,i}^{in} + \dot{H}_{g,i}^{f} + \dot{H}_{g,i}^{a} - \dot{H}_{g,i}^{out} + \dot{Q}_{g,i}. \quad (19)$$

Here, the enthalpy flow $\dot{H}_{g,i}^{in}$ defines the incoming bulk flow (cf. Fig. 3), $\dot{H}_{g,i}^{f}$ and $\dot{H}_{g,i}^{a}$ are related to the enthalpy flow of the fuel and the combustion air, the outgoing bulk flow is denoted by $\dot{H}_{g,i}^{out}$, and $\dot{Q}_{g,i}$ corresponds to the net heat flow into the gas volume. The net heat flow $\dot{Q}_{g,i}$ includes all thermal interactions of the flue gas and the surrounding surfaces, i.e., radiation and convection, and is coupled to the other net heat flows into the wall ($\dot{Q}_{w,i}$), the strip ($\dot{Q}_{s,i}$), and the guiding rolls ($\dot{Q}_{r,i}$) in the volume zone i in the following way $\dot{Q}_{g,i} + \dot{Q}_{w,i} + \dot{Q}_{s,i} + \dot{Q}_{r,i} = 0$. The relation between $H_{g,i}$ and the absolute (specific) enthalpy h^{ν} of the component ν is defined by

$$H_{g,i} = M_i h_{g,i}(T_{g,i}) \quad (20)$$

with $h_{g,i}(T_{g,i}) = \sum_{\nu \in \mathcal{S}} \xi_i^{\nu} h^{\nu}(T_{g,i})$. The remaining terms in (19) can be expressed as

$$\dot{H}_{g,i}^{in}(T_{g,i-1}) = \dot{M}_i^{in} \sum_{\nu \in \mathcal{S}} \xi_{i-1}^{\nu} h^{\nu}(T_{g,i-1}) \quad (21a)$$

$$\dot{H}_{g,i}^{f}(T_i^{f}) = \dot{M}_i^{f} h^{f}(T_i^{f}) \quad (21b)$$

$$\dot{H}_{g,i}^{a}(T_i^{a}) = \dot{M}_i^{a} h^{a}(T_i^{a}) \quad (21c)$$

$$\dot{H}_{g,i}^{out}(T_{g,i}) = \dot{M}_i^{out} \sum_{\nu \in \mathcal{S}} \xi_i^{\nu} h^{\nu}(T_{g,i}), \quad (21d)$$

with the absolute enthalpy $h^{\nu}(T)$ of the component $\nu \in \mathcal{S}$ at the temperature T, the absolute enthalpy $h^{f}(T^{f}) = h^{\mathrm{CH_4}}(T^{f})$ of $\mathrm{CH_4}$ at the fuel temperature T^{f}, and the absolute enthalpy $h^{a}(T^{a}) = \xi^{a,\mathrm{O_2}} h^{\mathrm{O_2}}(T^{a}) + \xi^{a,\mathrm{N_2}} h^{\mathrm{N_2}}(T^{a})$ of the combustion air at the air temperature T^{a}. The mass fractions of $\mathrm{O_2}$ and $\mathrm{N_2}$ with regard to the combustion air are defined by $\xi^{a,\mathrm{O_2}}$ and $\xi^{a,\mathrm{N_2}}$, which are coupled to the molar mass in the following way

$$\xi^{a,\mathrm{O_2}} = \frac{\bar{M}^{\mathrm{O_2}}}{\bar{M}^{\mathrm{O_2}} + 3.76 \bar{M}^{\mathrm{N_2}}} \quad (22a)$$

$$\xi^{a,\mathrm{N_2}} = \frac{3.76 \bar{M}^{\mathrm{N_2}}}{\bar{M}^{\mathrm{O_2}} + 3.76 \bar{M}^{\mathrm{N_2}}}. \quad (22b)$$

In each volume zone i, the temperature of the outgoing bulk flow is equal to the homogeneous gas temperature $T_{g,i}$, due to the assumption of a well stirred vessel.

Inserting (20) into (19) yields

$$M_i c_{p,g_i} \frac{\mathrm{d}T_{g,i}}{\mathrm{d}t} = \dot{H}_{g,i}^{in} + \dot{H}_{g,i}^{f} + \dot{H}_{g,i}^{a} - \dot{H}_{g,i}^{out} + \dot{Q}_{g,i}$$
$$- \frac{\mathrm{d}M_i}{\mathrm{d}t} h_{g,i}(T_{g,i}) - M_i \sum_{\nu \in \mathcal{S}} \frac{\mathrm{d}\xi_i^{\nu}}{\mathrm{d}t} h^{\nu}(T_{g,i}) \quad (23)$$

with the specific heat capacities $c_{p,g_i} = \sum_{\nu \in \mathcal{S}} \xi_i^{\nu} c_{p,g_i}^{\nu}$ and $c_{p,g_i}^{\nu} = \partial h^{\nu} / \partial T_{g,i}$. Eq. (23) is simplified to

$$M_i c_{p,g_i} \frac{\mathrm{d}T_{g,i}}{\mathrm{d}t} = \dot{M}_i^{in} \sum_{\nu \in \mathcal{S}} \xi_{i-1}^{\nu} h^{\nu}(T_{g,i-1}) + \dot{M}_i^{f} h^{\mathrm{CH_4}}(T_i^{f})$$
$$+ \dot{M}_i^{a} h^{a}(T_i^{a}) - \dot{M}_i^{in} \sum_{\nu \in \mathcal{S}} \xi_{i-1}^{\nu} h^{\nu}(T_{g,i})$$
$$- \dot{M}_i^{cb} \sum_{\nu \in \mathcal{S}} \xi_i^{\nu,cb} h^{\nu}(T_{g,i}) + \dot{Q}_{g,i} \quad (24)$$

by considering (13a), (16), and (21).

For the analysis of chemical reaction systems, it is often useful to split the absolute (specific) enthalpy $h^{\nu}(T)$ of a component $\nu \in \mathcal{S}$ in the latent heat $\tilde{h}_l^{\nu}$ and the sensible heat $\Delta\tilde{h}_s^{\nu}(T)$, i.e.,

$$h^{\nu}(T) = \tilde{h}_l^{\nu} + \Delta\tilde{h}_s^{\nu}(T). \quad (25)$$

The latent heat $\tilde{h}_l^{\nu}$ can be determined by tabulated values of standard enthalpy of formation. $\mathrm{H_2}$, $\mathrm{O_2}$, and $\mathrm{N_2}$ exist as diatomic molecules, hence $\tilde{h}_l^{\mathrm{H_2}} = \tilde{h}_l^{\mathrm{O_2}} = \tilde{h}_l^{\mathrm{N_2}} = 0$ [41]. The sensible heat $\Delta\tilde{h}_s^{\nu}(T)$ corresponds to a temperature change with respect to a reference temperature T_{ref}, with $\Delta\tilde{h}_s^{\nu}(T_{ref}) = 0$. The sensible heat can be determined by $\Delta\tilde{h}_s^{\nu}(T) = \bar{c}_{p,g}^{\nu}(T)(T - T_{ref})$, where $\bar{c}_{p,g}^{\nu}(T)$ is the average specific heat capacity at constant pressure [41].

Similarly to (21), the following abbreviations for the sensible heat corresponding to the bulk flows are introduced:

$$\Delta\dot{H}_{g,i}^{in}(T_{g,i-1}) = \dot{M}_i^{in} \sum_{\nu \in \mathcal{S}} \xi_{i-1}^{\nu} \Delta\tilde{h}_s^{\nu}(T_{g,i-1}) \quad (26a)$$

$$\Delta\dot{H}_i^{f}(T_i^{f}) = \dot{M}_i^{f} \Delta\tilde{h}_s^{\mathrm{CH_4}}(T_i^{f}) \quad (26b)$$

$$\Delta\dot{H}_i^{a}(T_i^{a}) = \dot{M}_i^{a} \Delta\tilde{h}_s^{a}(T_i^{a}). \quad (26c)$$

9

The sensible heat, which leaves the volume zone i, is given by

$$\Delta \dot{H}_{g,i}^{out}(T_{g,i}) = \dot{M}_i^{in} \sum_{\nu \in \mathcal{S}} \xi_{i-1}^{\nu} \Delta \tilde{h}_s^{\nu}(T_{g,i})$$
$$+ \dot{M}_i^{cb} \sum_{\nu \in \mathcal{S}} \xi_i^{\nu,cb} \Delta \tilde{h}_s^{\nu}(T_{g,i}). \quad (26d)$$

Using (25), (26), and $\dot{M}_i^{cb} \xi_i^{\nu,cb} = \dot{M}_i^f \chi_i^{\nu} \bar{M}^{\nu} / \bar{M}^{CH_4}$ in (24) yields

$$M_i c_{p,g_i} \frac{dT_{g,i}}{dt} = \Delta \dot{H}_{g,i}^{in}(T_{g,i-1}) + \Delta \dot{H}_i^f(T_i^f) + \Delta \dot{H}_i^a(T_i^a)$$
$$- \Delta \dot{H}_{g,i}^{out}(T_{g,i}) + \dot{H}_L + \dot{Q}_{g,i} \quad (27)$$

with the latent heat

$$\dot{H}_L = \dot{M}_i^f \left(\tilde{h}_l^{CH_4} - \sum_{\nu \in \mathcal{S}} \frac{\bar{M}^{\nu}}{\bar{M}^{CH_4}} \chi_i^{\nu} \tilde{h}_l^{\nu} \right). \quad (28)$$

In (28), the expression set in parenthesis is also known as calorific value. The number of moles of component $\nu \in \mathcal{S}$ in volume zone i is given by χ_i^{ν}, which is related to the combustion of CH_4, and is defined by (3) and (5) (cf. Sec. 2.1.2). The evolution of the flue gas temperature can be determined by (27); it depends on the sensible heat terms (26) and on the latent heat (28).

2.2. The furnace wall

Figure 5: Furnace section with a moving strip.

Fig. 5 shows a sectional view of the furnace duct. The furnace wall consists of N_w layers and each

layer j is parameterized by the mass density $\rho_{w,j}$, the specific heat capacity $c_{w,j}$, the thermal conductivity $k_{w,j}$, and the thickness $d_{w,j}$. The surface temperatures of the wall at the inner and outer side are T_{wI} and T_{wO}. It is assumed that T_{wO} equals the constant ambient temperature, i.e., a Dirichlet boundary condition is used. For the inner surface, a Neumann boundary condition with the heat flux $\dot{q}_w = \dot{Q}_w / S_w$ is assumed, where $\dot{Q}_w$ is the total heat flow into a wall section with the surface area S_w. Therefore, the wall temperature $T_w(\eta,t)$ can be described by the one-dimensional heat conduction equation [1, 20, 21]

$$\rho_w(\eta) c_w(\eta) \frac{\partial T_w(\eta,t)}{\partial t} = \frac{\partial}{\partial \eta} \left(k_w(\eta) \frac{\partial T_w(\eta,t)}{\partial \eta} \right)$$
$$0 < \eta < d_w, t > t_0, \quad (29a)$$

with the local mass density ρ_w, the local specific heat capacity c_w, and the local thermal conductivity k_w. For the considered layered wall, these material parameters are piecewise constant. The initial condition

$$T_w(\eta,t_0) = T_{w,0}(\eta), \quad 0 \le \eta \le d_w \quad (29b)$$

and the boundary conditions

$$T_w(d_w,t) = T_{wO}, \quad t > t_0 \quad (29c)$$

$$\dot{q}_w = -k_w(\eta) \left. \frac{\partial T_w(\eta,t)}{\partial \eta} \right|_{\eta=0}, \quad t > t_0, \quad (29d)$$

complete (29a). To obtain a low dimensional and computationally efficient lumped parameter system, (29) is spatially discretized by means of the Galerkin weighted residual method [11, 34, 47]. Therefore, it is assumed that the temperature profil can be approximated by

$$\hat{T}_w(\eta,t) = v(\eta) T_{wI}(t) + (1 - v(\eta)) T_{wO}, \quad (30)$$

where $v(\eta)$ is an appropriate trial function that satisfies $v(0) = 1$ and $v(d_w) = 0$. Note that the time dependency is captured by T_{wI}, which is the so-called Galerkin coefficient. An approximate solution of the heat conduction equation (29) results in an ordinary differential equation of the wall, which

is given by

$$\frac{\mathrm{d}T_{wI}}{\mathrm{d}t} = \frac{1}{K_{w1}}\dot{q}_w + \frac{K_{w2}}{K_{w1}}(T_{wO} - T_{wI}) \qquad (31)$$

with the initial condition $T_{wI}(t_0) = T_{wI,0}$ corresponding to (29b) and the constants K_{w1} and K_{w2}. These constants are defined as

$$K_{w1} = \int_0^{d_w} \rho_w(\eta)c_w(\eta)v^2(\eta)\mathrm{d}\eta \qquad (32a)$$

$$K_{w2} = \int_0^{d_w} k_w(\eta)\left(\frac{\partial v(\eta)}{\partial \eta}\right)^2 \mathrm{d}\eta. \qquad (32b)$$

A reasonable choice of the trial function $v(\eta)$ is obtained by analyzing the stationary solution of the heat conduction equation for a multi-layered furnace wall. It can be found by equalizing the heat fluxes through the individual layers and is given, for instance, in [20].

2.3. Strip

Since the Biot number Bi [20] is much smaller than one ($Bi \ll 1$), the strip temperature can be considered as homogeneous along the direction y (cf. Fig. 5). Furthermore, it is assumed that the strip with the width b_s and the thickness d_s moves along the direction z in the center of the furnace duct with the velocity v_s, which may vary with the time t.

Lagrangian or Eulerian coordinates are used for the description of the system variables and properties associated with the strip. The Lagrangian coordinate $\tilde{z}$ is fixed to a given material point, whereas the Eulerian coordinate z is spatially fixed. The relation between Lagrangian and Eulerian coordinates is given by

$$z = \tilde{z} + \int_{t_0}^{t} v_s(t')\mathrm{d}t', \qquad (33)$$

which implies $z = \tilde{z}$ for $t = t_0$. For the analysis of the strip temperature, an infinitesimal strip section of the length $\mathrm{d}z_s > 0$ is considered (cf. Fig. 5). The local heat fluxes into the strip section as indicated in Fig. 5 are defined by $\dot{q}_s^-$ and $\dot{q}_s^+$. It is assumed that $\dot{q}_s = \dot{q}_s^- = \dot{q}_s^+$ because the furnace has a symmetrical design. Based on the heat balance, the dynamic behavior of the strip temperature $\tilde{T}_s(\tilde{z},t)$ in Lagrangian coordinates reads as

$$\frac{\mathrm{d}\tilde{T}_s(\tilde{z},t)}{\mathrm{d}t} = \frac{2\dot{q}_s(\tilde{z},t)}{\rho_s c_s(\tilde{T}_s(\tilde{z},t))d_s} \qquad (34a)$$

with the initial condition $\tilde{T}_s(\tilde{z},t_0) = \tilde{T}_{s,0}(\tilde{z})$ and the heat flux $\dot{q}_s(\tilde{z},t)$ in Lagrangian coordinates, which will be computed later.

The Eulerian counterpart of (34a) reads as

$$\frac{\partial T_s(z,t)}{\partial t} = \frac{2\dot{q}_s(z,t)}{\rho_s c_s(T_s(z,t))d_s} - v_s \frac{\partial T_s(z,t)}{\partial z}, \quad (34b)$$

with the initial condition $T_s(z,t_0) = \tilde{T}_{s,0}(z)$ and the boundary condition $T_s(0,t) = \tilde{T}_{s,0}\left(-\int_{t_0}^{t} v_s(t')\mathrm{d}t',t\right)$. In (34), the specific heat capacity c_s depends on the temperature and also on the material (though the argument $\tilde{z}$ is not explicitly shown in (34)). In (34b), the transport term can be discretized by means of finite differences [12, 37, 42]. In case of Lagrangian coordinates, the strip is discretized into $\tilde{N}_s$ finite sections with the lengths $\Delta\tilde{z}_i = \tilde{z}_{i-1} - \tilde{z}_i, i = 1,...,\tilde{N}_s$, where the position of the i-th section in Lagrangian coordinates is defined as $\tilde{z}_i$. If Eulerian coordinates are used for the discretization, the strip is partitioned into $\bar{N}_s$ finite sections with the lengths $\Delta z_j = z_{j-1} - z_j, j = 1,...,\bar{N}_s$, where z_j defines the position of the discretized section in Eulerian coordinates.

In the following, a mapping of the strip temperatures and the local heat fluxes is presented. In Sec. 2.6, the zone method [27] will be used for the calculation of the radiative heat transfer. It requires a spatial discretization of the furnace and assumes a constant temperature for each surface and volume zone. Moreover, it yields the heat flows to these surface zones. The spatial discretization is kept constant to minimize the computational effort, i.e., it is given in Eulerian coordinates. However, since the strip is generally represented in a Lagrangian framework, a mapping scheme is introduced for the strip temperature and the heat flows used in (34a).

In the following, the abbreviations $\tilde{T}_{s,i}(t) = \tilde{T}_s(\tilde{z}_i,t)$ and $T_{s,j}(t) = T_s(z_j,t)$ will be used for simplicity. $T_{s,j}(t)$ is assumed to be uniform within a surface

11

section (z_j, z_{j-1}). The relation

$$T_{s,j}(t) = \frac{1}{\Delta z_j} \int_{z_j}^{z_{j-1}} \tilde{T}_s \left(z - \int_{t_0}^{t} v_s(t') \mathrm{d}t', t \right) \mathrm{d}z \quad (35)$$

$$\forall j = 1, \ldots, \bar{N}_s$$

maps the strip temperature from Lagrangian coordinates to Eulerian coordinates. This temperature is now representative for the temperature on the position $z_j + \Delta z_j/2$. The integral with respect to z is approximated by a numerical quadrature and results in a linear mapping $\mathbf{T}_s = \mathbf{M}_T \tilde{\mathbf{T}}_s$ with $\mathbf{T}_s = [T_{s,1}, ..., T_{s,\bar{N}_s}]^T$, $\tilde{\mathbf{T}}_s = [\tilde{T}_{s,1}, ..., \tilde{T}_{s,\bar{N}_s}]^T$ and the temperature mapping matrix $\mathbf{M}_T$.

Following the zone method, the local heat flux in Eulerian coordinates is piecewise constant, so that the abbreviation $\dot{q}_{s,j}(t) = \dot{q}_s(z,t)\big|_{z \in [z_j, z_{j-1}]}$ can be used. The following relation transfers these values to Lagrangian coordinates

$$\dot{\tilde{q}}_{s,i}(t) = \dot{\tilde{q}}_{s,i}(\tilde{z}_i, t) =$$
$$\frac{1}{\Delta \tilde{z}_i} \int_{\tilde{z}_i}^{\tilde{z}_{i-1}} \dot{q}_s \left(\tilde{z} + \int_{t_0}^{t} v_s(t') \mathrm{d}t', t \right) \mathrm{d}\tilde{z} \quad (36)$$

$$\forall i = 1, \ldots, \tilde{N}_s.$$

Here, $\tilde{q}_{s,i}(t)$ defines the heat flux into the discretized strip section i in Lagrangian coordinates. A linear mapping in the form $\dot{\tilde{\mathbf{q}}}_s = \mathbf{M}_q \dot{\mathbf{q}}_s$ is given by a numerical quadrature of (36), where $\dot{\tilde{\mathbf{q}}}_s = [\dot{\tilde{q}}_{s,1}, ..., \dot{\tilde{q}}_{s,\tilde{N}_s}]^T$, $\dot{\mathbf{q}}_s = [\dot{q}_{s,1}, ..., \dot{q}_{s,\tilde{N}_s}]^T$ and $\mathbf{M}_q$ is the local heat flux mapping matrix.

2.4. Roll

The strip is conveyed through the furnace by means of three guiding rolls (cf. Fig. 1). Since the thermal inertia of the rolls has a nonnegligible influence on the strip temperature, they are modeled as lumped parameter systems, each with homogeneous temperature $T_r(t)$.

Let M_r be the mass and c_r the temperature-dependent specific heat capacity of a single roll. Based on the heat balance, the ordinary differential equation for the roll temperature $T_r(t)$ follows as

$$\frac{\mathrm{d}T_r(t)}{\mathrm{d}t} = \frac{\dot{Q}_r}{M_r c_r(T_r(t))}, \quad (37)$$

with the initial condition $T_r(t_0) = T_{r,0}$ and the total heat flow $\dot{Q}_r$ into the roll. This heat flow summarizes the heat exchange with the flue gas, the wall,

and the strip by thermal radiation (cf. Sec. 2.6), convection (cf. Sec. 2.5), and conduction. Conduction occurs due to the mechanical contact between the roll and the strip and can be modeled by

$$\dot{Q}_{r,con} = S_{con} \frac{T_s - T_r}{R_{con}}, \quad (38)$$

with the local strip temperature T_s, the contact area $S_{con} = d_r \pi b_s / 4$ between the roll and the strip, the diameter of the roll d_r, and the thermal contact resistance R_{con} [7, 20]. Eq. (38) can be rewritten in vector-matrix notation as follows

$$\dot{\mathbf{Q}}_{r,con} = \mathbf{S}_{con} \dot{\mathbf{q}}_{r,con} = \mathbf{S}_{con} \mathbf{R}_{con}^{-1} \left(\mathbf{\Gamma}_{con} \mathbf{T}_s - \mathbf{T}_r \right), \quad (39)$$

where $\mathbf{S}_{con} = \mathrm{diag}\left(S_{con,1}, S_{con,2}, S_{con,3} \right)$ defines the diagonal matrix of the contact areas and $\mathbf{R}_{con} = \mathrm{diag}\left(R_{con,1}, R_{con,2}, R_{con,3} \right)$ the diagonal matrix of the thermal contact resistances. The matrix $\mathbf{\Gamma}_{con}$ selects the temperatures of the strip, which are in contact with the roll. In (39), $\dot{\mathbf{Q}}_{r,con} = [Q_{r,con,1}, Q_{r,con,2}, Q_{r,con,2}]^T$ is the vector of the conductive heat flows and the vector $\mathbf{T}_r = [T_{r,1}, T_{r,2}, T_{r,3}]^T$ defines the vector of the three roll temperatures. Moreover, the matrix $\mathbf{\Xi}_{con}$ can be considered as a selection matrix, which maps the three dimensional vector $\dot{\mathbf{q}}_{r,con}$ to an $\tilde{N}_s$ dimensional vector (cf. Fig. 7).

2.5. Convective heat transfer

For the considered furnace, the assumption of forced convection seems justified because of the bulk flow of the flue gas as well as the strip motion. The convective net heat flow between a fluid with the free stream temperature T_{fluid} and a solid with the surface temperature T_{solid} and the surface area S_c can be modeled by *Newton's law of cooling*

$$\dot{Q}_c = S_c h_c \left(T_{fluid} - T_{solid} \right), \quad (40)$$

where h_c is the convection heat transfer coefficient, which depends on the conditions in the boundary layers [1, 20, 21, 22], e.g., fluid motion, surface geometry, and thermal properties.

The convection heat transfer coefficient h_c can be determined from the Nusselt number [20, 22]

$$Nu = \frac{h_c l}{k_f}. \quad (41)$$

12

Here, l is the length of the considered flat surface and k_f is the thermal conductivity of the fluid. The Nusselt number Nu describes the ratio between convective and conductive heat transfer across the thermal boundary layer and can be computed by the empirical relation [1, 20]

$$Nu = 0.68 Re^{1/2} Pr^{1/3} \qquad (42)$$

with the Reynolds number $Re = \rho_g w_\infty l / \mu_g$, and the Prandtl number $Pr = \mu_g c_{p,g} / k_f$. The relative velocity between the free stream of the fluid and the surface is defined by w_∞, the dynamic viscosity of the fluid is μ_g, ρ_g is the density of the fluid, and $c_{p,g}$ denotes the specific heat capacity. Based on the Eqs. (41) – (42), the unknown parameter h_c can be determined.

By considering the direct-fired furnace, *Newton's law of cooling* in vector-matrix notation yields

$$\dot{\mathbf{Q}}_c = \mathbf{S}_c \mathbf{h}_c \left(\mathbf{T}_g^c - \mathbf{T}^c \right). \qquad (43)$$

Now, the vector of the convective heat flow is defined as $\dot{\mathbf{Q}}_c = \left[Q_{c,w_1}, \ldots, Q_{c,w_N}, Q_{c,r_1}, Q_{c,r_2}, Q_{c,r_3}, Q_{c,s_1}, \ldots, Q_{c,s_{\bar{N}_s}} \right]^T$, where the first N elements of the vector define the convective heat exchange between the flue gas and the wall, followed by heat flow between the flue gas and the roll, and final the $\bar{N}_s$ heat flows between the flue gas and the strip. The matrices $\mathbf{S}_c$ and $\mathbf{h}_c$ have a diagonal structure, where $\mathbf{S}_c$ contains the surface areas of the walls, the rolls, and the strip, respectively. The matrix $\mathbf{h}_c$ includes the respective convective heat transfer coefficients. All surface temperatures are included in the vector $\mathbf{T}^c = \left[T_{wI,1}, \ldots, T_{wI,N}, T_{r,1}, T_{r,2}, T_{r,3}, T_{s,1}, \ldots, T_{s,\bar{N}_s} \right]^T$. To describe the convective heat transfer of the flue gas with the surrounding, the vector $\mathbf{T}_g^c$ is defined as $\mathbf{T}_g^c = \mathbf{\Psi}_c \mathbf{T}_g$, where $\mathbf{\Psi}_c$ is a mapping matrix. Furthermore, a matrix $\mathbf{\Lambda}_c$ is required, which maps the vector $\dot{\mathbf{Q}}_c$ to a vector of the dimension N (cf. Fig. 8).

2.6. Radiative heat transfer

Due to the high temperatures inside the considered strip annealing furnace, thermal radiation is the dominant mode of heat transfer. Since the flue gas contains molecules with non-symmetrical oscillation patterns, e.g., H_2O and CO_2 (cf. [21, 27]),

the flue gas has to be considered as a participating medium.

In contrast to convection and conduction, thermal radiation is a global phenomenon in the sense that it depends on surface temperatures and material properties of distant points. A comfortable way to model the radiative heat transfer is the zone method [27, 30, 31]. It was first proposed by Hottel and coworkers [16].

A general thermal radiation problem is shown in Fig. 6, where a multi-surface enclosure contains a homogeneously distributed participating gas. It is assumed that the surfaces and the gaseous medium act like diffuse gray radiators. For applying the zone method, the enclosure is divided into N_s surface sections and the gas volume is divided into N_g subvolumes. The surface section $k = 1, \ldots, N_s$ is characterized by the surface area S_k, an emissivity coefficient ϵ_k [30, 31], and the surface temperature T_k. Furthermore, a subvolume $l = 1, \ldots, N_g$ is supposed to have the volume V_l, the gas temperature $T_{g,l}$, and the attenuation coefficient K_l [27, 30, 31]. The value $1/K_l$ can be interpreted as the main free path of a photon until it is absorbed by the gaseous medium. The
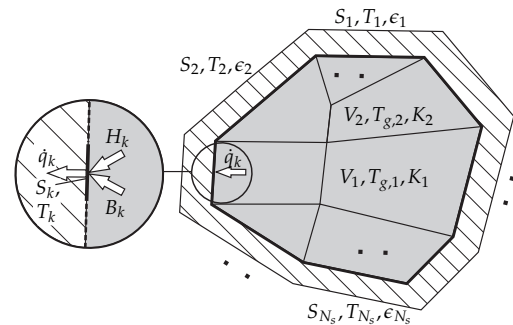

Figure 6: Multi-surface enclosure.

net radiative heat flows $\dot{\mathbf{Q}}_{rad} = [\dot{Q}_1, \ldots, \dot{Q}_{N_s}]^T = \mathrm{diag}\{\mathbf{S}\}\, \dot{\mathbf{q}}_{rad} = \mathrm{diag}\{\mathbf{S}\}[\dot{q}_1, \ldots, \dot{q}_{N_s}]^T$ into the surface sections and $\dot{\mathbf{Q}}_{g,rad} = [\dot{Q}_{g,rad,1}, \ldots, \dot{Q}_{g,rad,N_g}]^T$ into the subvolumes, respectively, can be expressed by

$$\dot{\mathbf{Q}}_{rad} = \mathbf{P}_{ss} \mathbf{T}^4 + \mathbf{P}_{sg} \mathbf{T}_g^4, \qquad (44a)$$

$$\dot{\mathbf{Q}}_{g,rad} = \mathbf{P}_{gs} \mathbf{T}^4 + \mathbf{P}_{gg} \mathbf{T}_g^4, \qquad (44b)$$

13

with $\mathbf{T}^4 = \left[T_1^4, ..., T_{N_s}^4 \right]^T$, $\mathbf{T}_g^4 = \left[T_{g,1}^4, ..., T_{g,N_g}^4 \right]^T$ and the surface area vector $\mathbf{S} = [S_1, ..., S_{N_s}]^T$. The matrices $\mathbf{P}_{ss}$, $\mathbf{P}_{sg}$, $\mathbf{P}_{gs}$, and $\mathbf{P}_{gg}$ depend on the Stefan-Boltzmann constant, the emissivity factors, the attenuation coefficient, and the so-called direct-exchange areas [30, 31], which in general are obtained by solving high dimensional integrals. For the furnace under consideration the direct-exchange areas have been computed by means of a semi-empirical approximation for rectangular geometries [32]. The matrices $\mathbf{P}_{ss}$, $\mathbf{P}_{sg}$, $\mathbf{P}_{gs}$, and $\mathbf{P}_{gg}$ can be calculated offline and directly result from the application of the zone method.

2.7. Assembled state space model

The building blocks of the mathematical model of the direct-fired continuous strip annealing furnace, which have been discussed in the previous sections, are now assembled. Using the heat transfer relations (38), (40), and (44), the ordinary differential equations (16), (27), (31), (34), and (37) can be rewritten in the compact form

$$\frac{\mathrm{d}}{\mathrm{d}t} \begin{bmatrix} \boldsymbol{\zeta} \\ \mathbf{T}_g \\ \mathbf{T}_w \\ \mathbf{T}_r \\ \mathbf{T}_s \end{bmatrix} = \begin{bmatrix} \mathbf{f}_\zeta \left(t, \boldsymbol{\zeta}, \mathbf{u} \right) \\ \mathbf{f}_{T_g} \left(t, \boldsymbol{\zeta}, \mathbf{T}_g, \mathbf{T}_w, \mathbf{T}_r, \mathbf{T}_s, \mathbf{u} \right) \\ \mathbf{f}_{T_w} \left(t, \mathbf{T}_g, \mathbf{T}_w, \mathbf{T}_r, \mathbf{T}_s \right) \\ \mathbf{f}_{T_r} \left(t, \mathbf{T}_g, \mathbf{T}_w, \mathbf{T}_r, \mathbf{T}_s \right) \\ \mathbf{f}_{T_s} \left(t, \mathbf{T}_g, \mathbf{T}_w, \mathbf{T}_r, \mathbf{T}_s \right) \end{bmatrix}, \quad (45)$$

with the state vector $\mathbf{x} = \left[\boldsymbol{\zeta}^T, \mathbf{T}_g^T, \mathbf{T}_w^T, \mathbf{T}_r^T, \mathbf{T}_s^T \right]^T$ and the abbreviation $\mathbf{f}(t, \mathbf{x}, \mathbf{u}) = \left[\mathbf{f}_\zeta^T, \mathbf{f}_{T_g}^T, \mathbf{f}_{T_w}^T, \mathbf{f}_{T_r}^T, \mathbf{f}_{T_s}^T \right]^T$. The total mass M_i and the mass flow $\dot{M}_i^{out}$ are given by (17), (18), and (13a).

The inputs are merged into the vector $\mathbf{u} = \left[\mathbf{u}_1^T, ..., \mathbf{u}_N^T \right]^T$. In the four HZs $n = 4, ..., 7$, the input vector $\mathbf{u}_n$ contains the mass flow of the fuel $\dot{M}_n^f$, the respective fuel temperature T_n^f, the mass flow of the combustion air $\dot{M}_n^a$, the air temperature T_n^a, and the strip velocity v_s. In the PCC, the input vector $\mathbf{u}_n$ only consists of the mass flow of the air $\dot{M}_n^a$, and the air temperature T_n^a. For the remaining volume zones, the strip velocity v_s is the only input.

In (45), $\boldsymbol{\zeta}$ summarizes the gas concentrations of the individual volume zones, i.e., $\boldsymbol{\zeta} = [\boldsymbol{\zeta}_1^T, ..., \boldsymbol{\zeta}_N^T]^T$ with $\boldsymbol{\zeta}_n = [\tilde{\zeta}_n^{CO_2}, \tilde{\zeta}_n^{CO}, \tilde{\zeta}_n^{H_2}, \tilde{\zeta}_n^{H_2O}, \tilde{\zeta}_n^{O_2}, \tilde{\zeta}_n^{N_2}]^T$ and

$n = 1, ..., N$. The flue gas in the transition zone bottom contains $\{H_2, N_2\}$, in the HZs and in the transition zone top it consists of $\{CO_2, CO, H_2O, H_2, N_2\}$, and in the PCC and in the PH it basically comprises $\{CO_2, H_2O, O_2, N_2\}$. The use of all components $\nu \in \mathcal{S}$ in the vector $\boldsymbol{\zeta}_n$ entails one redundant differential equation for each volume zone, which is omitted for a more efficient computer implementation.

The temperatures of the flue gas and the inner wall surfaces in the N volume zones are summarized in $\mathbf{T}_g = [T_{g,1}, ..., T_{g,N}]^T$ and $\mathbf{T}_w = [T_{wI,1}, ..., T_{wI,N}]^T$, respectively. $\mathbf{T}_r = [T_{r,1}, T_{r,2}, T_{r,3}]^T$ contains the roll temperatures. The dimension of the vector of the strip temperatures $\mathbf{T}_s = [\tilde{T}_{s,1}, ..., \tilde{T}_{s,\tilde{N}_s}]^T$ varies if Lagrangian coordinates are used (cf. (34a)). In the Eulerian framework (cf. (34b)), the dimension of $\mathbf{T}_s = [T_{s,1}, ..., T_{s,\bar{N}_s}]^T$ is constant.

As will be outlined in Sec. 3.1, the model can be divided into a fast and a slow subsystem. Since the thermal inertias of the wall, the rolls, and the strip are significantly higher than those of the gaseous media, the furnace wall, the rolls, and the strip constitute the slow subsystem. The composition and the temperature of the flue gas represent the fast subsystem. Fig. 7 shows the structure of the dynamical model of the wall, the roll, and the strip.

The inputs of the dynamical subsystems describing the strip, the rolls, and the walls are the heat fluxes $\dot{\mathbf{q}}_s$, $\dot{\mathbf{q}}_r$ and $\dot{\mathbf{q}}_w$. The most significant nonlinearity is the 4th–power, which is related to thermal radiation. Further nonlinearties come into play via the material parameters, i.e., the specific heat capacities c_r and c_s. The flue gas temperature $\mathbf{T}_g$ belongs to the fast subsystem and can thus be considered as an input for the slow subsystem. Note that the slow subsystem is independent of the gas concentration $\boldsymbol{\zeta}$ (cf. Fig. 7).

The structure of the flue gas dynamics (cf. (16) and (27)), which constitutes the fast subsystem, is outlined in Fig. 8. Here, the nonlinear behavior is characterized by (27), where the net heat flow $\dot{Q}_{g,i}$ contains the nonlinearity of the 4th–power due to thermal radiation (cf. Sec. 2.1.4). Since the differential equations of the composition and the temperature of the flue gas of volume zone i require the composition and the temperature of
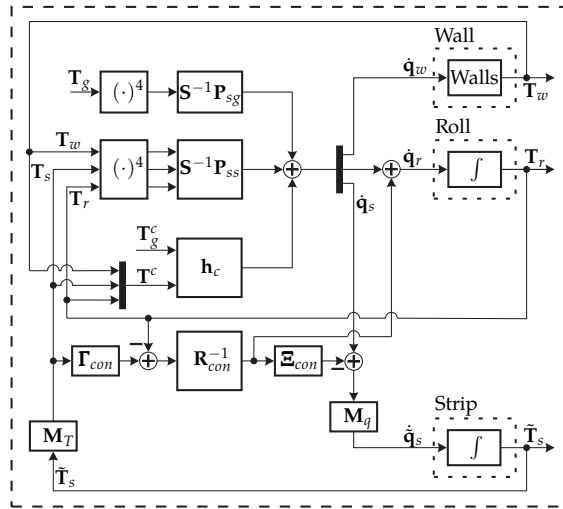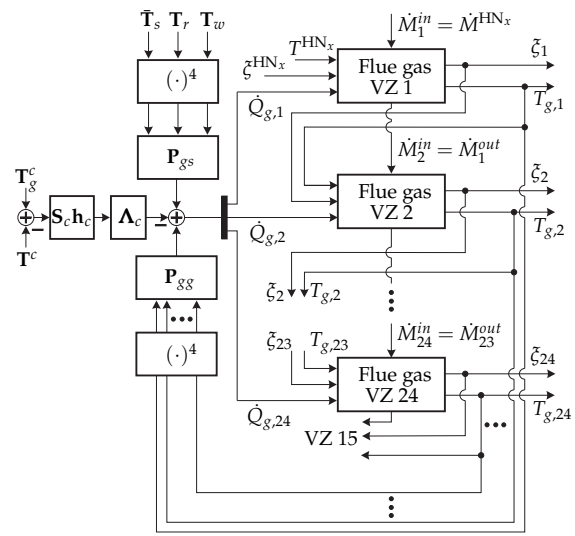
14

Figure 7: Structure of the wall, roll, and strip dynamics (Lagrangian coordinates).
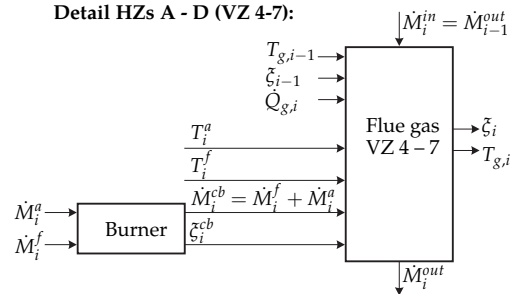

Detail HZs A - D (VZ 4-7):

Detail PCC (VZ 23):
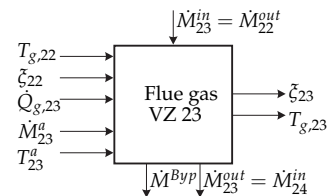
Figure 8: Structure of the flue gas dynamics.
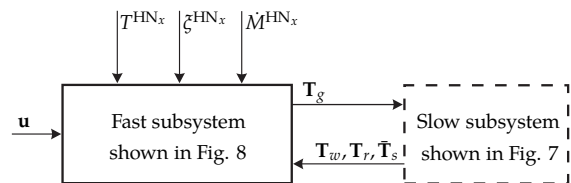
Figure 9: Structure of the quasi-steady-state model.

the previous volume zone $i-1$ this submodel has a cascade structure. In the first volume zone, the composition ξ^{HN_x}, the mass flow $\dot{M}_1^{in} = \dot{M}^{\mathrm{HN}_x}$, and the temperature T^{HN_x} of the incoming inert gas from the indirect-fired furnace serve as additional inputs. Note that the structure of the volume zones $8, 15, 20$ and 21 is not the same as in Fig. 8, because they are influenced by further mass and energy flows and not only by one incoming and one outgoing bulk flow.

Furthermore, Fig. 8 shows the structure of the flue gas dynamics in the HZs A – D (VZ 4 - 7) and in the PCC. In the PCC, additional combustion air enters the furnace volume through an air intake, which is characterized by the mass flow $\dot{M}_{23}^a$ and the temperature T_{23}^a.

Finally, the overall structure of the furnace model is depicted in Fig. 9, which indicates the interaction between the slow and the fast subsystem as outlined in Fig. 7 and Fig. 8, respectively. The input of the slow subsystem is the flue gas temperature $\mathbf{T}_g$ (cf. Fig. 9). If the flue gas dynamics is considered as quasi-stationary, the fast subsystem can be characterized by an algebraic equation that depends on the system input $\mathbf{u}$. This will be shown in the following section.

15

3. Model order reduction and time discretization

3.1. Reduced model

Based on Tikhonov's singular perturbation theory [24], a system comprising a fast and a slow subsystem, referred to with the state vectors $\mathbf{z}_1$ and $\mathbf{z}_2$, can be written in the standard form

$$\dot{\mathbf{z}}_1 = \tilde{\mathbf{f}}_1\left(t, \mathbf{z}_1, \mathbf{z}_2, \mathbf{u}, \kappa\right), \tag{46a}$$

$$\kappa \dot{\mathbf{z}}_2 = \tilde{\mathbf{f}}_2\left(t, \mathbf{z}_1, \mathbf{z}_2, \mathbf{u}, \kappa\right), \tag{46b}$$

with a small (dimensionless) singular perturbation parameter κ, the input vector $\mathbf{u}$, and the sufficiently smooth functions $\tilde{\mathbf{f}}_1$ and $\tilde{\mathbf{f}}_2$. If $\kappa \to 0$, the fast subsystem can be simplified to an algebraic equation of the form

$$0 = \tilde{\mathbf{f}}_2\left(t, \check{\mathbf{z}}_1, \check{\mathbf{z}}_2, \mathbf{u}, 0\right). \tag{47}$$

If (47) has an isolated root and can be solved at least numerically to obtain $\check{\mathbf{z}}_2 = \tilde{\mathbf{g}}\left(t, \check{\mathbf{z}}_1, \mathbf{u}\right)$, (46a) can be replaced by the so-called quasi-steady-state model

$$\dot{\mathbf{z}}_1 = \tilde{\mathbf{f}}_1\left(t, \check{\mathbf{z}}_1, \tilde{\mathbf{g}}\left(t, \check{\mathbf{z}}_1, \mathbf{u}\right), \mathbf{u}, 0\right). \tag{48}$$

The singular perturbation theory is now applied to the assembled state space model (45) of the considered direct-fired furnace. Based on a linearization of (45), a numerical analysis of the eigenvalues of the system has been made. This analysis has revealed the existence of a slow and a fast subsystem, i.e., the eigenvalues are clustered into two distinct groups. From the corresponding eigenvectors, it can be inferred that $\boldsymbol{\zeta}$ and $\mathbf{T}_g$ belong to the fast subsystem and $\mathbf{T}_w$, $\mathbf{T}_r$, and $\mathbf{T}_s$ to the slow subsystem. This is also plausible from a physical point of view.

The singular perturbation parameter κ is given by a product of mass and heat capacity values of the strip. The stability of the boundary layer model has not been rigorously proven due to the complexity and dimension of the mathematical model.

Based on the singular perturbation theory, the flue gas dynamics can be considered quasi-stationary cf. (16) and (27), i.e.

$$\begin{bmatrix} \mathbf{0} \\ \mathbf{0} \end{bmatrix} = \begin{bmatrix} \mathbf{f}_{\tilde{\zeta}}\left(t, \check{\boldsymbol{\zeta}}, \mathbf{u}\right) \\ \mathbf{f}_{T_g}\left(t, \check{\boldsymbol{\zeta}}, \check{\mathbf{T}}_g, \check{\mathbf{T}}_w, \check{\mathbf{T}}_r, \check{\mathbf{T}}_s, \mathbf{u}\right) \end{bmatrix}. \tag{49}$$

The remaining differential equations in (45) constitute the fast subsystem

$$\frac{\mathrm{d}}{\mathrm{d}t} \begin{bmatrix} \check{\mathbf{T}}_w \\ \check{\mathbf{T}}_r \\ \check{\mathbf{T}}_s \end{bmatrix} = \begin{bmatrix} \mathbf{f}_{T_w}\left(t, \check{\mathbf{T}}_g, \check{\mathbf{T}}_w, \check{\mathbf{T}}_r, \check{\mathbf{T}}_s\right) \\ \mathbf{f}_{T_r}\left(t, \check{\mathbf{T}}_g, \check{\mathbf{T}}_w, \check{\mathbf{T}}_r, \check{\mathbf{T}}_s\right) \\ \mathbf{f}_{T_s}\left(t, \check{\mathbf{T}}_g, \check{\mathbf{T}}_w, \check{\mathbf{T}}_r, \check{\mathbf{T}}_s\right) \end{bmatrix}. \tag{50}$$

For a compact notation, (49) and (50) are rewritten in the form

$$0 = \mathbf{f}_2\left(t, \check{\mathbf{z}}_1, \check{\mathbf{z}}_2, \mathbf{u}\right) \tag{51a}$$

$$\dot{\check{\mathbf{z}}}_1 = \mathbf{f}_1\left(t, \check{\mathbf{z}}_1, \check{\mathbf{z}}_2\right), \tag{51b}$$

with $\check{\mathbf{z}}_1 = [\check{\mathbf{T}}_w^T, \check{\mathbf{T}}_r^T, \check{\mathbf{T}}_s^T]^T$ and $\check{\mathbf{z}}_2 = [\check{\boldsymbol{\zeta}}^T, \check{\mathbf{T}}_g^T]^T$.

3.2. Time discretization

For computer implementation, e.g., in simulation, control, and optimization, (51) must be discretized with respect to the time t. Since (51) does not generally allow an analytical solution, a numerical integration by Euler's explicit and implicit method is employed.

Let t_k be the discretized time and $\Delta t_k = t_{k+1} - t_k$ the sampling time, which need not be equidistant. With $\check{\mathbf{z}}_{1,k} = \check{\mathbf{z}}_1(t_k)$ and $\check{\mathbf{z}}_{2,k} = \check{\mathbf{z}}_2(t_k)$ Euler's explicit method yields

$$0 = \mathbf{f}_{2,k}\left(\check{\mathbf{z}}_{1,k}, \check{\mathbf{z}}_{2,k}, \mathbf{u}_k\right) \tag{52a}$$

$$\check{\mathbf{z}}_{1,k+1} = \check{\mathbf{z}}_{1,k} + \Delta t_k \mathbf{f}_{1,k}\left(\check{\mathbf{z}}_{1,k}, \check{\mathbf{z}}_{2,k}\right). \tag{52b}$$

By means of Netwon's method, (52a) can be solved for $\check{\mathbf{z}}_{2,k}$ independently from (52b). The choice of the sampling time Δt_k turns out to be critical for the numerical stability of the integration method. In particular, if the formulation (34b) (Eulerian reference frame with finite difference approximation of the transport term) is used, small sampling times are indispensible.

The implicit Euler method permits significantly larger sampling times; in fact, the method is unconditionally stable [36]. However, the additional computational effort is not rewarded by considerably better numerical properties, which is why Euler's explicit method is applied henceforth.

The sampling time is also influenced by the choice of the spatial discretization of the strip. If the Eulerian framework is used, the Courant-Friedrichs-Lewy (CFL) condition [15] has to be fullfilled. This

16

condition is given by

$$\Delta t_k < \frac{\Delta z}{v_s}, \tag{53}$$

where v_s is the strip velocity and $\Delta z = \min(\Delta z_j)$, $j = 1,...,\bar{N}_s$ denotes the minimum spatial discretization size of the strip (cf. Sec. 2.3). In case of the Lagrangian framework, a condition like the CFL condition does not exist. In the simulation, each material point should capture the influence of each volume zone (heat flux) to ensure a sufficiently high accuracy. Therefore, the maximum sampling time $\Delta t_k = l_{fur}/v_s$ is used, where l_{fur} defines the minimum length of all volume zones and depends always on the minimum contact length of the rolls.

In [38], a comparison between Eulerian and Lagrangian coordinates is presented. Compared to the Eulerian framework, the Lagrangian coordinates are more efficient regarding the CPU time and more accurate regarding the temperature resolution at welded joints. Therefore, the following validation is based on the Lagrangian description.

4. Measurement results and model validation

For parameter identification and model validation, a measurement campaign was conducted on the considered direct-fired strip annealing furnace that is part of a hot-dip galvanizing line of voestalpine Stahl GmbH, Linz, Austria. For this purpose, the measurement equipment already installed in the furnace was sufficient. Thermocouples measure the flue gas and the wall temperature in the furnace and two pyrometers are used to measure the strip temperature at two discrete points (cf. Fig. 1). Since the strip temperature is the most important process quantity, the model was mainly validated by means of the pyrometer P2. The system inputs, i.e., the mass flows of fuel and air, their temperatures, and the extra air inflow in the PCC, are also known from measurements. The measurement values are compared to simulation results obtained from a MATLAB/SIMULINK implementation of the proposed model (51). In the simulation, the strip is spatially discretized with a step size of 0.5m in the Lagrangian framework.

4.1. Parameter identification

In general, each parameter of the derived model has a clear physical meaning. Since some of these parameters are not exactly known, e.g., the structure of the wall in the PCC and the emissivity of the strip, they are identified based on measured data. For the PCC, the unknown parameter $K_{w1,23}$ in (31) can be found from the optimization problem

$$K_{w1,23}^{opt} = \underset{K_{w1,23}}{\arg\min} J_1 \tag{54}$$

with the cost function

$$J_1 = \sqrt{\frac{1}{t_e - t_b} \int_{t_b}^{t_e} \left(T_{g,23}(t) - \Theta_{g,PCC}(t)\right)^2 \mathrm{d}t}, \tag{55}$$

where t_b and t_e are the start and end time, $T_{g,23}(t)$ represents the simulated flue gas temperature in the PCC, and $\Theta_{g,PCC}(t)$ is the corresponding thermocouple measurement. Note that the calculated value J_1 can be interpreted as a temperature error. Fig. 10 indicates how the cost function J_1 depends on $K_{w1,23}$ and Fig. 11 shows the good
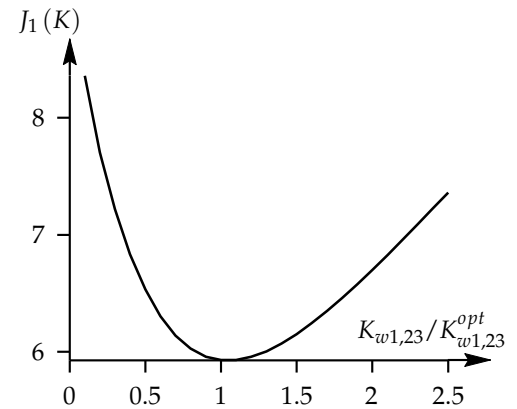
Figure 10: Cost function J_1.

agreement between $\Theta_{g,PCC}(t)$ and $T_{g,23}(t)$ simulated with $K_{w1,23}^{opt}$.

Generally, the emissivity coefficient ε_s of the strip depends on the local strip temperature and varies from product to product. Since the measurement of ε_s is a sophisticated task, an average strip emissivity value is identified and used for all products.
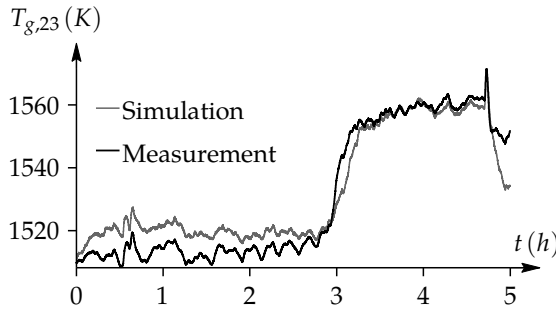
17

Figure 11: Comparison of simulated and measured gas temperatures in the PCC (volume zone 23).

The identified value for ε_s is found from the optimization problem

$$\varepsilon_s^{opt} = \arg\min_{\varepsilon_s} J_2 \qquad (56)$$

with the cost function

$$J_2 = \sqrt{\frac{1}{t_e - t_b} \int_{t_b}^{t_e} \left(T_{s,P2}(t) - \Theta_{s,P2}(t)\right)^2 \mathrm{d}t} \qquad (57)$$

that is shown in Fig. 12. Here, $T_{s,P2}(t)$ is the simulated strip temperature at the position of the pyrometer P2 and $\Theta_{s,P2}(t)$ is the corresponding measured time evolution. The obtained optimal value
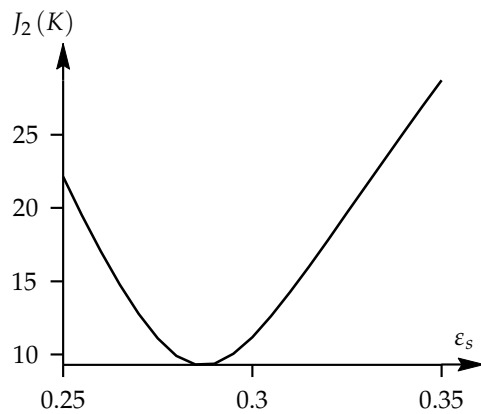
Figure 12: Cost function J_2.

is $\epsilon_s^{opt} \approx 0.29$.

4.2. Validation

The model is validated by comparing simulation results with measurements obtained from the industrial strip annealing furnace. It is worth noting that the measurement data for the identification is different from the data used for model validation. In the considered measurement cam-
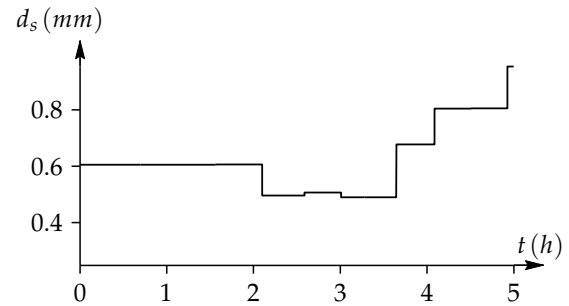
Figure 13: Strip thickness.
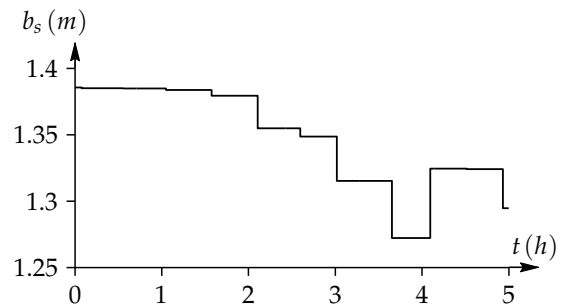
Figure 14: Strip width.

paign, the strip moved with a velocity v_s in the range of $1.7 - 2.7\,\mathrm{m/s}$, had a width b_s between $1.27 - 1.39\,\mathrm{m}$ (cf. Fig. 14), and a strip thickness d_s in the range of $0.5 - 1.0\,\mathrm{mm}$ (cf. Fig. 13). Moreover, the strip temperature is influenced by the density and the specific heat capacity of the strip [14]. As mentioned in Sec. 2.3, the specific heat capacity depends on the strip temperature T_s, see Fig. 15. Throughout this work, the constant strip density $\rho_s = 7800\,kg/m^3$ is used. The same specific heat capacity and density of the strip was used for all steel grades. If the strip parameters were known with higher accuracy, the quality of the mathematical model could be further improved. Fig. 16 shows the measured and the simulated strip temperature
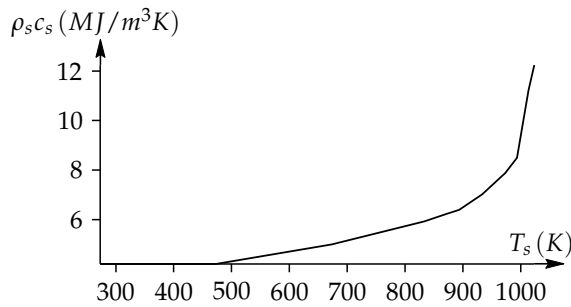
18

Figure 15: Product of strip density and specific heat capacity.

at the end of the furnace, i.e., at the pyrometer P2. Generally, the figure shows that a good accuracy can be achieved by the model. The sudden
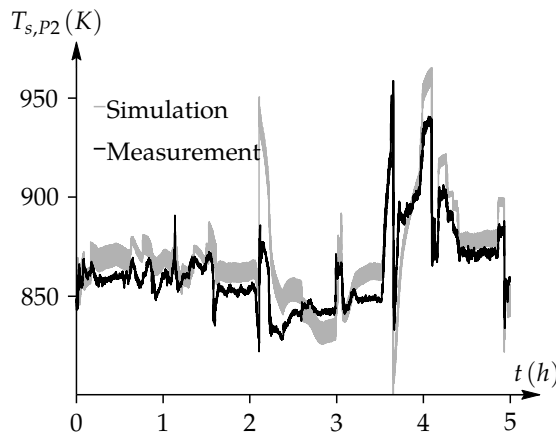

Figure 16: Strip temperature at pyrometer P2.

changes of the strip temperature are mainly caused by changes of the strip properties, i.e., transitions of products (cf. Fig. 13). For some strips, a lack of accurate knowledge of the material properties causes a considerable model mismatch. For example, the simulated strip temperature decreases whereas the measured strip temperature even rises at the time $t \approx 2.5\,\mathrm{h}$. The simulated temperature drop is plausible because the strip thickness increases at this time (cf. Fig. 13). This model mismatch is thus mainly related to the uncertain emissivity coefficient of the strip. This is also why we aim at developing an online estimator for the emissivity coefficient in our future work. Furthermore, the rise of the simulated strip temperature at the time $t \approx 2.0\,\mathrm{h}$

is much higher than the measured temperature. This effect can be explained with a change in the steel grade. In fact, the material parameters of the corresponding strip are not exactly known.

The flue gas temperature $T_{g,23}$ of the PCC is shown in Fig. 17. The simulated results match the measured time evolutions. The flue gas temperature $T_{g,23}$ is significantly influenced by the combustion of unburnt gas components. Based on these results, it can be concluded that the combustion is well captured by the proposed mathematical model. The legend of Fig. 16 also applies to Figs. 17 – 21.

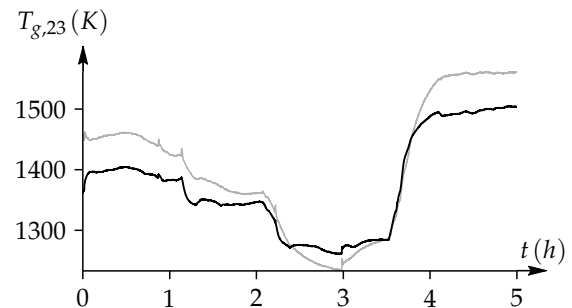Figs. 18 - 21 depict the results of the model in

Figure 17: Flue gas temperature in the PCC.

terms of the wall temperatures in the four HZs. The figures corroborate that the dynamic behavior of the HZs is well captured by the model.

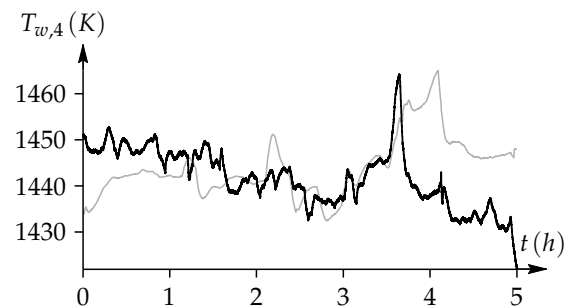Finally, in Fig. 22 the simulated strip tem-

Figure 18: Wall temperature in the HZ 1.

perature trajectory of a material point that moves through the furnace is presented. The location of the rolls is also shown in Fig. 22. The heating of the strip mainly occurs in the HZs and also in
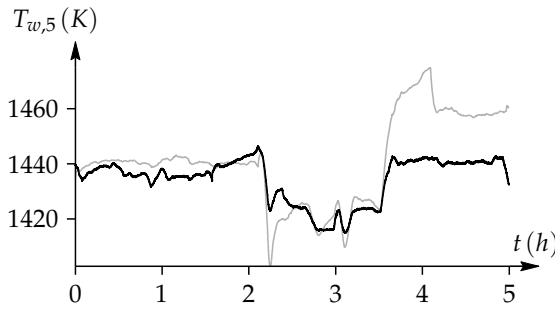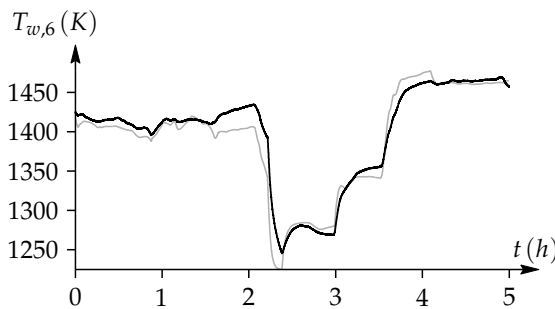
19

the PH. In both transition zones, the strip temperature is nearly constant. Furthermore, the influence

$T_{w,5}\,(K)$

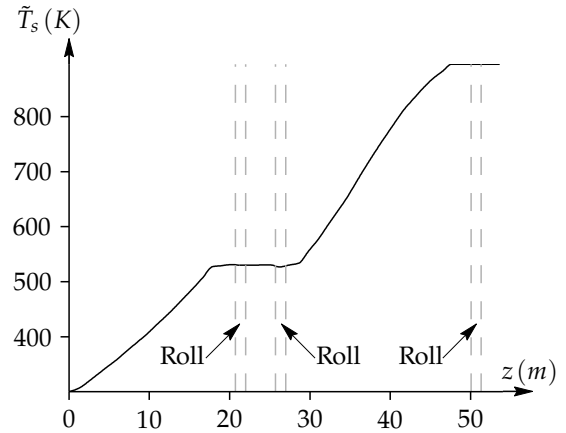Figure 19: Wall temperature in the HZ 2.

$\tilde{T}_s\,(K)$

Figure 22: Strip temperature through the furnace.

of the rolls has been investigated in more detail. For this, two different simulations have been conducted; one by considering the rolls and the second one by neglecting the rolls. In Fig. 23, the difference of the strip temperature trajectories $\Delta\tilde{T}_s$ is presented. Neglecting the rolls raises the strip temperature at the end of the furnace by approximately 5.5 K.

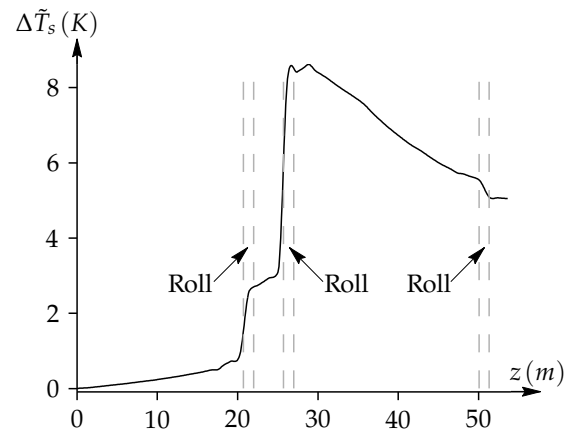The considered mathematical model was imple-

$T_{w,6}\,(K)$

Figure 20: Wall temperature in the HZ 3.

$\Delta\tilde{T}_s\,(K)$

Figure 23: Difference between the strip temperature trajectory by neglecting the rolls and by considering the rolls.

$T_{w,7}\,(K)$

Figure 21: Wall temperature in the HZ 4.

mented and simulated on a standard PC (3.6 GHz, 4.0 GB RAM) with variable sampling time Δt_k in

20

the range of $0.45 - -0.65\,\mathrm{s}$. On this system, the simulation of the considered 5 h scenario requires approximately 9 min CPU time. The obtained results show that the mathematical model is suitable for real-time control applications.

5. Conclusions

In this work, a tractable, first-principles model of a direct-fired strip annealing furnace was developed with a focus on applications in model-based control and optimization. The furnace was divided into N volume zones. Due to the fuel-rich combustion of the natural gas, the water-gas-shift reaction was considered to determine the mass fractions of the chemical products under quasi-steady-state conditions. The enthalpy balance made it possible to calculate the flue gas temperature. The Galerkin method was employed for the discretization of the 1-dimensional heat conduction equation of the wall. This approximation yields an ordinary differential equation for the furnace wall. Based on the heat balance, the dynamic behavior of the strip temperature was determined. Depending on the choice of Eulerian or Lagrangian coordinates, the dynamic behavior of the strip is either described by a partial differential equation with a transport term or by an ordinary differential equation. Furthermore, the dynamic behavior of the temperature of the deflecting rolls was also calculated by means of the heat balance. In addition, thermal conduction between the strip and the rolls was taken into account. Convective and radiative heat transfer connect the various thermal submodels. The zone method was utilized for the determination of the radiative heat transfer.

To make the model suitable for real-time applications, it was reduced by means of the singular perturbation theory. Euler's explicit method was used for time discretization with an adaptive selection of sampling times. For the numerical simulation, the assembled model was implemented in Matlab/Simulink.

The proposed model was validated by comparing measurements from the considered continuous strip annealing furnace with simulation results.

The main advantages of the proposed mathematical model are its scalability, the achieved accuracy, the low computational effort, and the adequate consideration of nonlinear effects like thermal radiation, temperature-dependent material parameters, and the chemical reactions.

References

[1] H.D. Baehr and K. Stephan. *Heat and mass transfer*. Springer-Verlag: Berlin Heidelberg, 2nd edition, 2006.

[2] S. Banerjee, D. Sanyal, S. Sen, and I.K. Puri. A methodology to control direct-fired furnaces. *International Journal of Heat and Mass Transfer*, 47(24):5247–5256, 2004.

[3] L. Bitschnau and M. Kozek. Modeling and control of an industrial continuous furnace. In *Proceedings of the International Conference on Computational Intelligence, Modelling and Simulation (CSSim)*, pages 231–236, Brno, Czech Republic, September 2009.

[4] P. Boineau, C. Copin, and F. Aguile. Heat transfer modelling using advanced zone model based on a CFD code. In *Proceedings of the 6th European Conference on Industrial Furnaces and Boilers (INFUB)*, pages 88–94, Lisbon, Portugal, May 2002.

[5] S.R. Carvalho, T.H. Ong, and G. Guimaraes. A mathematical and computational model of furnaces for continuous steel strip processing. *Journal of Materials Processing Technology*, 178:379–387, 2006.

[6] Y.A. Cengel and J.M. Cimbala. *Fluid mechanics*. McGraw-Hill Book Company: New York, 2nd edition, 2009.

[7] T.-C. Chen, C.-H. Ho, J.-C. Lin, and L.-W. Wu. 3-D temperature and stress distributions of strip in preheating furnace of continuous annealing line. *Journal of Applied Thermal Engineering*, 30:1047–1057, 2010.

[8] Y. Choi and H.G. Stenger. Water gas shift reaction kinetics and reactor modeling for fuel cell grade hydrogen. *Journal of Power Sources*, 124:432–439, 2003.

[9] J. Dai, Q. Zhang, and T. Chang. FEM analysis of large thermo-deflection of strips being processed in a continuous annealing furnace. *Journal of University of Science and Technology Beijing*, 14(6):580–584, 2007.

[10] N. Depree, J. Sneyd, S. Taylor, M.P. Taylor, J.J.J. Chen, S. Wang, and M. O'Connor. Development and validation of models for annealing furnace control from heat transfer fundamentals. *Journal of Computers and Chemical Engineering*, 34(11):1849–1853, 2010.

[11] C.A.J. Fletcher. *Computational Galerkin Methods*. Springer-Verlag: Berlin Heidelberg, 16th edition, 1984.

[12] E. Godlewski and P.-A. Raviart. *Numerical Approximation of Hyperbolic Systems of Conservation Laws*, volume 118. Springer-Verlag: New York, 1996.

[13] J. Goyhénèche and J. Sacadura. The zone method: A new explicit matrix relation to calculate the total exchange areas in anisotropically scattering medium bounded by anisotropically reflecting walls. *Journal of Heat Transfer*, 124:696–703, 2002.

[14] E. Hanitzsch. Messung der spezifischen Wärmekapazität von Stählen nach der Pulsmethode. *Thermochimica Acta*, 119(1):203–210, 1987.

[15] M.H. Holmes. *Introduction to Numerical Methods in Differential Equations*. Springer-Verlag: New York, 2007.

[16] H.C. Hottel. *Radiant-Heat Transmission*. McGraw-Hill Book Company: New York, 3rd edition, 1954.

[17] H.C. Hottel and E.S. Cohen. Radiant heat exchange in a gas filled enclosure: Allowance for non-uniformity of gas temperature. *American Institute of Chemical Engineering Journal*, 4:3–14, 1958.

[18] H.C. Hottel and A.F. Sarofim. The effects of gas flow patterns on radiative transfer in cylindrical enclosures. *International Journal of Heat and Mass Transfer*, 8:1153–1169, 1965.

[19] T.A. Adams II and P. I. Barton. A dynamic two-dimensional heterogeneous model for water gas shift reactors. *International Journal of Hydrogen Energy*, 34:8877–8891, 2009.

[20] F.P. Incropera, D.P. Dewitt, T.L. Bergmann, and A.S. Lavine. *Fundamentals of heat and mass transfer*. John Wiley and Sons: Hoboken, New Jersey, 6th edition, 2007.

[21] J.H. Lienhard IV and J.H. Lienhard V. *A Heat Transfer Textbook*. Phlogiston Press: Cambridge, 3rd edition, 2008.

[22] W. Kay, M. Crawford, and B. Weigand. *Convective Heat and Mass Transfer*. McGraw-Hill Book Company: New York, 4th edition, 2005.

[23] C.D. Kelly, D. Watanapongse, and K.M. Gaskey. Application of modern control to a continuous anneal line. *IEEE Control Systems Magazine*, 8(2):32–37, 1988.

[24] P. Kokotovic, H.K. Khalil, and J. O'Reilly. *Singular pertubation methods in control*. Society for Industrial and Applied Mathematics (SIAM), Philadelphia, 1999.

[25] D. Marlow. *Mathematical modelling of the heat treatment in the continuous processing of steel strip*. PhD thesis, University of Wollongong, 1995.

[26] D. Marlow. Modelling direct-fired annealing furnaces for transient operations. *Applied Mathematical Modelling*, 20(1):34–40, 1996.

[27] M.F. Modest. *Radiative heat transfer*. Academic Press: San Diego, 2nd edition, 2003.

[28] J.M. Moe. Design of water-gas shift reactors. *Chemical Engineering Progress*, 58(3):33–36, 1962.

[29] M.J. Moran and H.N. Shapiro. *Fundamentals of Engineerings Thermodynamics*. John Wiley and Sons: Hoboken, New Jersey, 6th edition, 2010.

[30] J.M. Rhine and R.J. Tucker. *Modelling of gas-fired furnaces and boilers*. McGraw-Hill Book Company: New York, 1st edition, 1991.

[31] R. Siegel and J. Howell. *Thermal radiation heat transfer*. Taylor & Francis: New York, London, 4th edition, 2002.

[32] A. Steinboeck. *Model-based control and optimization of a continuous slab reheating furnace*. PhD thesis, Vienna University of Technology, Austria, Shaker :Aachen, 2011.

[33] A. Steinboeck, D. Wild, T. Kiefer, and A. Kugi. A mathematical model of slab reheating furnace with radiative heat transfer and non-participating gaseous media. *International Journal of Heat and Mass Transfer*, 53:5933–5946, 2010.

[34] A. Steinboeck, D. Wild, T. Kiefer, and A. Kugi. A fast simulation method for 1D heat conduction. *Mathematics and Computers in Simulation*, 82(3):392–403, 2011.

[35] A. Steinboeck, D. Wild, and A. Kugi. Nonlinear model predictive control of a continuous slab reheating furnace. *Control Engineering Practice*, 21(4):495–508, April 2013.

22

[36] J. Stoer and R. Burlisch. *Introduction to Numerical Analysis*. Springer-Verlag: New York, Berlin, Heidelberg, 3rd edition, 2002.

[37] J. Strikwerda. *Finite Difference Schemes and Partial Differential Equations*. Society for Industrial and Applied Mathematics (SIAM), Pacific Grove, CA, 2nd edition, 2004.

[38] S. Strommer, M. Niederer, A. Steinboeck, and A. Kugi. Computational model of a direct-fired continuous strip annealing furnace for simulation, control, and optimization. In *Proceedings of the 2012 European Congress on Computational Methods in Applied Sciences and Engineering (ECCOMAS)*, 2012.

[39] Y.-C. Tian, C.-H. Hou, and F. Gao. Mathematical model of a continuous galvanizing annealing furnace. *Developments in Chemical Engineerung and Mineral Processing*, 8:359–374, 2000.

[40] M.K. Tiwari, A. Mukhopadhyay, and D. Sanyal. Process modeling for control of a batch heat treatment furnace with low NO_x radiant tube burner. *Energy Conversion and Management*, 46:2093–2113, 2005.

[41] S.T. Turns. *An Introduction to Combustion*. McGraw-Hill Book Company: Singapore, 2nd edition, 2006.

[42] R. Vichnevetsky and J. Bowles. *Fourier Analysis of Numerical Approximations of Hyperbolic Equations*. Society for Industrial and Applied Mathematics (SIAM), 1982.

[43] D. Wild. *Modellierung und Beobachterentwurf für einen Stossofen*. PhD thesis, Vienna University of Technology, Austria, Shaker: Aachen, 2010.

[44] D. Wild, T. Meurer, and A. Kugi. Modelling and Experimental Model Validation for a Pusher-type Reheating Furnace. *Mathematical and Computer Modelling of Dynamical systems (MCMDS)*, 15(3):1–20, 2009.

[45] S. Xuegang, Y. Chao, and C. Yihui. Dynamic Modeling of Reheat-Furnace Using Neural Network based on PSO Algorithm. In *Proceedings of the 2009 IEEE International Conference on Mechatronics and Automation*, pages 3097–3101, Changchun, China, August 2009.

[46] N. Yoshitani. Modelling and parameter estimation for strip temperature control in continuous annealing processes. In *Proceedings of the International Conference on Industrial Electronics, Control, and Instrumentation (IECON)*, volume 1, pages 469–474, November 1993.

[47] O.C. Zienkiewicz and K. Morgan. *Finite Elements and Approximation*. John Wiley and Sons: Hoboken, New Jersey, 1983.

23